Metabolic Brain Disease (2023) 38:1581–1612
https://doi.org/10.1007/s11011-023-01185-8

ORIGINAL ARTICLE

Necrostatin-1S mitigates type-2 diabetes-associated cognitive decrement and lipotoxicity-induced neuro-microglia changes through p-RIPK-RIPK3-p-MLKL axis

Kumari Preeti[1] · Valencia Fernandes[1] · Anika Sood[1] · Islauddin Khan[1] · Dharmendra Kumar Khatri[1,2] · Shashi Bala Singh[1]

Received: 3 October 2022 / Accepted: 13 February 2023 / Published online: 10 March 2023

Abstract

Type-2 diabetes mellitus (T2DM) is associated with neuroinflammation and cognitive decrement. Necroptosis programmed necrosis is emerging as the major contributing factor to central changes. It is best characterized by the upregulation of p-RIPK(Receptor Interacting Kinase), p-RIPK3, and the phosphorylated-MLKL (mixed-lineage kinase domain-like protein). The present study aims to evaluate the neuroprotective effect of Necrostatin (Nec-1S), a p-RIPK inhibitor, on cognitive changes in the experimental T2DM model in C57BL/6 mice and lipotoxicity-induced neuro-microglia changes in neuro2A and BV2 cells. Further, the study also explores whether Nec-1S would restore mitochondrial and autophago-lysosomal function.T2DM was developed in mice by feeding them a high-fat diet (HFD) for 16 weeks and injecting a single dose of streptozotocin (100 mg/kg, i.p) on the 12th week. Nec-1S was administered for 3 weeks at (10 mg/kg, i.p) once every 3 days. Lipotoxicity was induced in neuro2A, and BV2 cells using 200 µM palmitate/bovine serum albumin conjugate. Nec-1S (50 µM), and GSK-872(10 µM) were further used to explore their relative effect. The neurobehavioral performance was assessed using mazes and task-assisted performance tests. To decipher the hypothesis plasma parameters, western blot, immunofluorescence, microscopy, and quantitative reverse transcription–PCR studies were carried out. The Nec-1S treatment restored cognitive performance and reduced the p-RIPK-p-RIPK3-p-MLKL mediated neuro-microglia changes in the brain and in cells as well, under lipotoxic stress. Nec-1S reduced tau, and amyloid oligomer load. Moreover, Nec-1S restored mitochondrial function and autophago-lysosome clearance. The findings highlight the central impact of metabolic syndrome and how Nes-1S, by acting as a multifaceted agent, improved central functioning.

Keywords Hyperlipidemia · Hyperglycemia · Hippocampus · Interleukin · Synapse · Microglia · Oligomer · Necrosome · Mitochondria

Introduction

Metabolic syndrome is a constellation of disorders related to an increased risk of cardiovascular disease and is the major contributor to the development of type 2 diabetes(T2DM) largely due to the unhealthy lifestyles of modern society(Gustafson and Mcfarlane 2018). There are 90% higher chances of AD in borderline T2DM, and as per the consensus, the prevalence in the number of T2DM patients going to see a rise from 108 million in 1980 to 422 million, a shift from 4.7% to 8.5% by 2050 (WHO) (Zilliox et al. 2016; Riederer et al. 2017). The blood-brain barrier (BBB) and resident immune cells like microglia and astrocyte protect neurons from the direct insult of peripheral inflammation, cardiovascular, aging, and age-related comorbidities. There is clinical evidence too, where the diabetic patient's brain has shown significant abnormality in MRI scans. Moreover, in trial studies, besides Type-1 and Type-2 DM subjects, High fat diet-fed mice were assessed for their cognitive performance and brain alteration via neuroimaging (Rollins et al. 2019; Frison et al. 2021) Surprisingly, all have validated the fact that diabetic subjects present different

✉ Dharmendra Kumar Khatri
dkkhatri10@gmail.com

✉ Shashi Bala Singh
sbsingh.dipas@gmail.com

[1] Department of Pharmacology and Toxicology, National Institute of Pharmaceutical Education, and Research (NIPER)-Hyderabad, Telangana 500037, India

[2] Molecular and Cellular Neuroscience Lab, Department of Pharmacology & Toxicology, National Institute of Pharmaceutical Education and Research (NIPER)-Hyderabad, Telangana 500037, India

extent of dementia and are more prone to Alzheimer's disease (AD) or vascular dementia (VD). Various population-based trial study in their respective geographical area has shown the prevalence of cognitive decline in diabetic subjects (Chakraborty et al. 2021; Junyi et al. 2022; Lin et al. 2022; Panyawattanakit et al. 2022). One of the recent guidelines has categorized memory impairment manifestation into 3 types namely, dementia, mild cognitive impairment, and diabetes-specific cognitive decrement (Biessels and Whitmer 2019).

There are various classical therapeutic alternatives such as thiazolidinediones, sulfonylureas, dipeptidyl peptidase-4 (DPP-4), and α-glucosidase inhibitors available for the treatment of T2DM. However later exhibits many drawbacks such as weight gain, and hypoglycemia and they don't exhibit protection against T2DM-associated complications such as neuropathy, nephropathy, and cognitive impairment (Rai et al. 2019). Meanwhile, there are newer alternatives like Glucagon-like Peptides (GLP-1, GLP-2) agonists are being investigated for their sustained antidiabetic effect and diabetes-associated long-term complications (Sharma et al. 2018). The involvement of oxidative stress, insulin resistance-mediated after-effects, neuronal apoptosis mitochondrial dysfunction, loss of neurotrophic support, epigenetic changes, and proteastasis concerning metabolic stress-mediated cognitive changes are well discussed in many places (Kuhad et al. 2009). Although antidiabetic drugs can control diabetes, they have not been able to prevent ongoing central changes. The diabetic brain is also linked with the deposition p-Tau, amyloid deposit, and AD-like hallmarks (Jeon et al. 2012; Li and Casanueva 2016).

Necroptosis, the programmed necrosis emerged as a mechanism that has been reported as the major contributing factor for age-related neuroinflammation (2021), endothelial dysfunction leading to BBB loss (Takechi et al. 2017; Zou et al. 2020), neurodegeneration in case of AD (Caccamo et al. 2017), Parkinson's disease (Iannielli et al. 2018), stroke, TBI, retinal degeneration, ischemic brain injury (Zhang et al. 2020). Apoptotic death has long been discussed as the prime mechanism causing neuronal death but the question of extensive neuroinflammation remained unanswered. Necroptosis is one such mechanism where the programmed death of a cell occurs, but in addition, causes inflammation as it bypasses the phagocytic removal of debris besides releasing the DAMPs (Death-associated membrane Proteins) (Goodall et al. 2016). The best-characterized mechanism of necroptosis involves RIPK1-induced activation of RIPK3 through the formation of RIPK1/RIPK3 or RIPK3/MLKL (Rodriguez et al. 2015) necrosomes, which in turn phosphorylate the pseudo-kinase MLKL, a substrate of RIPK3[8,10]. This phosphorylation facilitates MLKL oligomerization, which then translocates and damages the cell membrane, subcellular organelle like mitochondria, and lysosome(Frank et al. 2019). Later interacts with phosphatidylinositol phosphate (PIP) phospholipids, leading to mitochondrial uncoupling(Karch et al. 2015), autophagy loss(Frank et al. 2019), and eventually cell death (Li et al. 2021). The RIPK3 can also modulate other processes through apoptosis or cytokine production independent of MLKL. Meanwhile, p-RIPK3 regulates DRP-mediated Mito fission/fusion imbalance leading to an increase in mitochondrial fragmentation further exaggerating oxidative stress (Zhou et al. n.d.). Necrostatin (Nec-1S) is an extensively investigated small molecule as a modulator wherever necroptosis-related pathomechanism is being discussed. Additionally, Nec-1S has the potential to bind directly to the amyloid-beta (Aβ) aggregate as its architecture matches to necrosome and hence could further contribute to reducing the Aβ-mediated neurodegeneration progression (Yang et al. 2017). In the present work, we are hypothesizing that T2DM led to peripheral metabolic stress, and BBB derangement which ultimately led to the p-MLKL mediated neuronal death and disease-associated microglia (DAM) changes involving mitochondrial dysfunction, autophagic loss, and lysosomal defect. Considering all the previous necroptosis-related research, the present study firstly discusses standardizing T2DM-induced cognitive decrement in experimental mice and palmitate-bovine serum albumin (PA-BSA) conjugate induced neuroinflammation and DAM changes in Neuro2a and BV2 cells respectively. Further, if the cognitive decrement is presented by the mice, then whether the necroptosis-like changes were involved in neuron, DAM and DAA. The combined use of High fat diet (60% calorie from fat) and streptozotocin(STZ) induces T2DM in C57BL/6 mice are well reported by metabolic research community (Barrière et al. n.d.; Lu et al. 2018; Kim et al. 2020). Similarly, PA-BSA conjugate was used to mimic the T2DM associated obesity at cellular level to further explore the mechanistic changes (Kim et al. 2017; Melo et al. 2020). Nec-1S is used for their therapeutic potential and later GSK-872 also included in the present work to explore their relative effect on necrosome formation and its after effect.

Material and methods

Materials

Most of the chemicals used are of reagent grade and were procured from Sigma Aldrich (St. Louis, MO, USA), Himedia laboratories, and SRL Chemicals. High-Fat Diet (HFD) was obtained from VYAS Lab (Hyderabad, India). Streptozotocin was purchased from Sigma. Isoflurane was obtained from Raman 7 Weil Pvt. Ltd (Mumbai, India). Glucose oxidase-peroxidase, total cholesterol, low-density lipoprotein kit, high-density lipoprotein, and triglyceride, the kit was

purchased from Accurex (Mumbai, India). The insulin kit was purchased from MERK Millipore. TNF-α ELISA kit (Biolegend, CAT no) IL-6, IL-4, BDNF ELISA kit (R&D Systems: Products & Services for Cell Biology Research). Sodium Palmitate (P9767) and BSA (A9418) were obtained from Sigma Aldrich (St. Louis, MO, USA). JC-1(T3168) and Mitotracker (M7512) are obtained from Thermo fisher scientific, USA. Antibodies were obtained from CST, ABCAM, Santacruz, and Millipore. Necrostatin(Cat No-N1174) and GSK-872(6492/10) were procured from TCI chemicals and the R& D System. (Table 1).

Experimental design

This study was completed in 4 different experiments: 2 different *in vivo* on animals, and 2 different *in vitro* studies on N2A and BV2 cell line.

Study 1: Time course of developing T2DM and further the cognitive impairment
Study 2: Exploring the neuroprotective effect of Necrostatin
Study 3: Effect of palmitate-BSA conjugate on necroptosis mechanism and further assessment of the neuroprotective effect of Nec-1S and GSK-872 in N2A Cell
Study 4: Effect of palmitate-BSA conjugate on necroptosis mechanism and further assessment of microglial changes under the effect of Nec-1S in BV2 cell

Animal study 1

Study 1: Standardising the Type 2 diabetes-induced cognitive decrement

Animal studies were carried out as per the regulation of the Committee for the Purpose of Control and Supervision of Experiments on Animals (CPCSEA) and Institutional Animal Ethical Committee (IAEC)-NIPER-Hyderabad Telangana, India, and according to Animal Research Reporting of *In vivo* Experiments (ARRIVE) guidelines (du Sert et al. 2020), after getting approval of protocol no NIP/10/2019/PC/343. 8-week aged male C57BL/6 mice were procured and housed in polycarbonate cages (3–4 mice per cage) in a temperature-controlled room (22 ± 2 °C) with a 12 h light–dark cycle. They are allowed to feed on a normal pellet diet (NPD) and water ad libitum to get acclimatized in the institutional animal facility. Neuroscience research has been encouraging the inclusion of both male and female mice and should not be limited to any sex bias (Beery n.d.; Becker et al. 2016). However, the scientific conclusion of the present study has one circumstantial limitation as it has included only the male sex and could further be explored in female mice as well.

Induction of diabetes-induced cognition impairment and experimental design

Animals ($N = 40$) were weighed and randomized into different groups. Further, they were categorized into two groups i.e., NPD (Norm pellet diet, $n = 15$) and HFD (60% Kcal from fat, $n = 25$), and continued the same for a further 4 months/16 weeks. After 3 months of HFD single dose of 100 mg/kg STZ freshly prepared in chilled citrate buffer (pH 4.5) was administered intraperitoneal (Park et al. 2020). After 24 h of STZ administration, fasting blood glucose was examined by using a glucometer and commercially available Accurex kit. Once the hyperglycemia is confirmed animals were continued on HFD for further 4 weeks. Oral glucose tolerance test (OGTT) and intraperitoneal insulin tolerance test (IPTT) were performed to assess glucose tolerance and insulin insensitivity. Neurobehavioral studies were conducted for NPD-fed and HFD-fed to assess cognitive decrement after 16 weeks. The cognitive decrement was evident and further the animals were sacrificed for molecular studies. The 200 µl of blood was collected from the tail vein. Organs were collected by perfusing with Phosphate Buffer Saline (PBS) and PBS-PFA depending on the parameters

Table 1 Chemicals and supplier detail

Chemicals		
Necrostatin-1	TCI CHEMICALS	Cat No-N1174, CID: 2,828,334
GSK-872	R & D System	Cat No-6492/10, CID: 54,674,134
Streptozotocin	Sigma Aldrich	Cat No-6492/10,CID:57,654,595
Fluorescein sodium	Sigma Aldrich	Cat No-, F6377.CID: 24,894,907
Sodium Palmitate	Sigma Aldrich	Cat No-P9767, CID: 24,899,061
Experimental Model: Cell line		
N2A	NCCS PUNE, INDIA	RRID: CVCL_0470
BV2	E lab sciences	RRID: CVCL_0182)
Animal		
C57BL/6	Vyas lab	https://www.jax.org/strain/000664

to be evaluated. The brain, liver, pancreas, and kidney were isolated. Tissues were snap-frozen and preserved at -80 °C for further molecular studies(Fig. S.1A).

Study 2: Necrostatin administration

All the studies were carried out after getting approval from IAEC-NIPER-Hyderabad Telangana, India. After 16 weeks of diet manipulation, diabetic animals were further divided into 2 groups: T2DM + Veh, and T2DM + Nec-1S. Additionally, NPD-fed diet animals were considered NC. The dose of Nec-1S is based on a previous study (Iannielli et al. 2018; Qing et al. 2018) Necrostatin was administered for 3 weeks at (1st dose 10 mg/kg, i.p) once every 3 days. The drug stock was prepared in DMSO and further diluted in saline so that the final concentration of DMSO was < 2.5%. The study was exploratory and hence the endpoint was not predefined. After the completion of dosing, neurobehavioral parameters were evaluated, and organs and tissue were processed as mentioned earlier (Fig. 5A).

Biochemical measurement

To ensure that the animal exhibits T2DM characteristics, we have assessed Fasting Blood Glucose (FBG), Oral Glucose Tolerance Test (OGTT), and Intraperitoneal Insulin Tolerance Test (IPTT).

Fasting blood glucose

Blood was collected at 2:00 PM following a six-hour fast for metabolic measures. Blood glucose was measured using a glucometer. At the end of the study, FBG was also calculated using commercially available Accucheck kits.

Oral glucose tolerance test

In the oral glucose tolerance test, 20%-glucose was administered orally to mice. Glucose was estimated at the time intervals of 0, 15, 30, 60, and 90 min using the Accucheck glucometer. The glucose level at time intervals was plotted by applying 2-way ANOVA using a graph pad prism (Bowe et al. 2014).

Intraperitoneal insulin tolerance test

In the insulin sensitivity test, following 6 h. fast 0.8 units/kg of insulin (Novolin R, Novo Nordisk Pharmaceutical Industries, Inc.) was injected intraperitoneally. Glucose was estimated at the time interval of 0, 15, 30, 60, and 90 min using the Accucheck glucometer(Johnson et al. 2016).

Plasma lipid profile

Blood was collected in the heparinized tube and further centrifuged at 5000 rpm for 15 min. the plasma was collected and immediately the total cholesterol (TC), High-Density Lipoprotein (HDL), Low-density lipoprotein (LDL), total triglyceride (TG) was estimated using commercially available Accucheck kit. The rest of the plasma was stored at -80 °C.

Behavioral and cognitive analysis

Behavioral experiments were conducted by employing a blinding strategy. One of the co-authors who were not aware of the grouping has been involved during the experiment but not during the data analysis.

Y maze spontaneous exploratory memory test (assessing spatial working memory)

Spontaneous exploratory behavior was investigated by using a Y maze. The Y-maze apparatus consists of three arms, each 21 cm long, 4 cm wide, and 40 cm tall with a central entry zone. It is made of plastic and placed at an angle of 33°. Mice were placed individually in the central entry zone and allowed to rely on exploring the apparatus for 5 min while being recorded using ANY maze software. The total number of arm entries and alterations between the arms are recorded. Frequent exploration in all three arms indicates normal spontaneous exploration, whereas restricted arm entries indicate deficits in spontaneous exploration. Alternations were defined as successive entries into each of the three arms as on overlapping triplet sets (ABC, BCA, CAB…). The percent of spontaneous alternation performance was defined as the ratio of SAP to possible (total arm entries − 2) number of alternations × 100 (Yang et al. 2017; Rom et al. 2019).

Assessment of intermediate-term recognition memory: Novel Object Recognition (NORT)

Novel object recognition trials were conducted in square test boxes (40 × 40x35 cm) with even lighting conditions (30 ± 5 lx). Each test box consisted of a white Perspex bottom plate surrounded by black Perspex walls and a camera positioned centrally above each box. A white-painted round spherical bottle and a white-painted triangular bottle were used as objects. Before testing, mice were habituated for over 2 days(10 min each). On day 3 of the tests, a habituation trial was conducted where mice could explore the empty test box for 20 min. 24 h after the habituation trial (day 4 a sample trial was conducted. During the sample trial, mice were placed into the empty test box always in front of the south

wall facing away from the objects. After a 5 min customization phase, two equal sample objects were introduced into the box. The mouse was allowed to explore the objects for 10 min before it was returned to its home cage. After 60 min, NORT was conducted by placing the mouse into the empty test box again. After an initial 5 min customization phase, one sample object and one unfamiliar object were introduced, and object interaction was recorded for 10 min. Object interaction was defined as an event where a mouse's head was within 2 cm of the object and directed towards the object. percent time spent exploring the novel versus familiar object was calculated Johnson et al. 2016; Kodali et al. 2021).

Spatial learning and memory in the Morris water maze

We performed based on the reported method with some modifications The water maze, a circular pool (diameter 150 cm), filled with opaque water (Nonfat milk powder, 2 °C) divided into four quadrants. Mice were subjected to the training of 4 trials/day for 7 days, consisting of 2 days of visible followed by 5 days of the hidden platform. During visible training, the flagged platform was kept 1 cm above the water surface in absence of extra MAZE cues. Each mouse went through a 60-s trial and was removed from the pool after locating the platform and remaining on it 5 s. Mice were put into the maze at varying locations during each trial to avoid procedural bias. Meanwhile during the Visible Platform trials of task learning location of the platform was moved for each trial between the four quadrants to avoid procedural biases. During the hidden platform trial, mice were trained to locate the platform in presence of four extra maze cues placed at four quadrants for spatial reference and orientation. The platform was not rotated during the Hidden Platform trials but rather kept constant in the SW taken as the Target quadrant. After 24 h of the last trial, the probe trial was performed for 30 s where the platform was removed to assess spatial memory retention. All the activities were recorded using ANY-maze software (ANY-maze, version 6.1). The parameters like latency to find the platform(in a sec) and distance swam (cm) and the probe-trial parameter (number of entries to the target platform zone and time in quadrants were analyzed Nunez 2008; Johnson et al. 2016).

Aversive learning memory/ passive avoidance (step-through task)

After the MWM test, the step-through passive avoidance response was performed. The apparatus consisted of an illuminated and a dark compartment, separated by a vertical sliding door. A mouse was initially placed in the illuminated compartment, with its tail toward the dark compartment for 3 min for environmental adaptation. With the door opened, the mice could enter the dark compartment (mice instinctively prefer being in the dark). Following the mice completely entering the dark compartment, it was given an electric shock (36 V, DC). And thereafter the mice returned to their home cage. Training at (0 h) and 24 h was performed for 5 min as mentioned above and the test was repeated 24 h after the 2nd training. During the training and retention trials, the number of errors and the latency before the initial entry into the dark compartment within 5 min were recorded, respectively. The retention trails were set at a limit of 300 s of cutoff time(Liu et al. 2014; Johnson et al. 2016).

Blood–brain barrier permeability test using sodium fluorescein (NaF)

To estimate BBB permeability 10% sodium fluorescein (NaF) (cat No: F6377-100G, Sigma Aldrich) solution was injected *i.p*. It was allowed to perfuse in the whole body for 40–45 min. Mice were perfused with PBS followed by the PFA until the clear solution starts coming out. Blood was collected and serum was isolated after centrifugation. The brain was collected and homogenized in PBS. Following centrifugation, the supernatant was collected. An equal amount of trichloroacetic acid (TCA) was mixed both in serum and tissue samples to precipitate protein and further centrifuged to collect the supernatant. The supernatant was neutralized by using an equal amount of 5N NaOH (Sodium Hydroxide). Further, the level of NaF was estimated both in tissue and serum sample by measuring fluorescent intensity at the excitation-emission wavelength (360/585 nm). Further, the NaF permeability in the brain was represented as the serum-to-tissue ratio (*10 ^{2}) (Amenta et al. 2014; Rom et al. 2019).

Microscopy study

Perfused brains were further stored in PFA for 24 h. followed by preserving in the 15 and, then 30% sucrose. The brain is cut in between different coordinates using a brain matrix and frizzed in an OCT block, further, to carry out the coronal cryosection of various thicknesses ranging from, 25–30-micron sections. Sections taken on the slide were further processed for various stainings like immunofluorescences, fluorojade C, and Thioflavin staining.

Fluoro-Jade-C staining

The frozen brain section ($n=3$) was taken out from -20 °C and kept for drying. After three PBS washing sections were incubated for 15 min in 0.001% fluorojade-C (FJ-C) solution. Later the sections were washed again with PBS and blocked in 3% BSA for 1 h. After blocking the

sections were washed again followed by immersion in ammonium chloride solution for 10 min to quench the autofluorescence. Sections were further washed twice in PBS and dried at 55° C followed by mounting with DPX. Sections were visualized for FJ-C positive neurons at 10 × and 20 × magnification using a Nikon eclipse Ti2 Fluorescence microscope, Japan at Ex: 485, Em: 520 nm (Schmued et al. 2005).

Thioflavin-S staining

After drying frozen brain sections ($n = 3$) were stained with 500 mM of thioflavin S (Thio-S) dissolved in 50% ethanol for 7 min. The sections were then rinsed with 100, 95, and 70% ethanol and PBS successively and mounted with anti-fade mounting media (Thangavel et al. 2017; Yang et al. 2017). Sections were visualized for amyloid oligomer positivity at 10 × and 20 × magnification using Olympus- BX53 Fluorescence microscope at Ex: 485, Em: 520 nm (Schmued et al. 2005).

Cell Culture

Cell maintenance

BV2 and N2A cell lines were obtained from elab Science USA, & NCCS (Pune, India) respectively, and used between passages number 5–16. Cells were cultured in DMEM-High glucose media supplemented with 10% FBS, and Streptomycin/Penicillin (1%). They were cultured at 37 °C, in a humidified atmosphere of 95% air, and 5% CO2 (Marwarha et al. 2016; Urso and Zhou 2021). Cells were authenticated by Neu-N staining for N2A and IBA staining for BV2 cells.

Palmitate conjugate preparation

Sodium Palmitate stock of 100 mM was prepared in sterile water and by heating at 70 °C. The 5% endotoxin-free BSA (sigma) stock in media was prepared. The final conjugate of 5 mM PA-BSA conjugate was prepared freshly before use in a 1:20 ratio and filtered through a 0.2 µm syringe filter (Kim et al. 2017).

Cell viability test

Palmitate dose Cells were incubated with different concentrations of PA-BSA conjugate ranging from 50-400 µM for 12 and 24 h at 37 °C and 5% CO2 followed by incubating with MTT for 3–4 h for cell death estimation. The cell survival was calculated as a percentage of survival and plotted.

Nec-1 s Cells were incubated with varied concertation of Necrostatin (Nec-1S) (6.25 µM—200 µM) at 37 °C and 5% CO2 followed by incubating with MTT for 3–4 h for cell death estimation. The cell survival was calculated as a percentage of survival and plotted.

GSK-872 Cells were incubated with varied concertation of GSK-872 (80–1.25 µM) at 37 °C and 5% CO2 followed by incubating with MTT for 3–4 h for cell death estimation. The cell survival was calculated as a percentage of survival and plotted.

Mitochondrial membrane potential (Ψm) (JC1 assay)

The cells were seeded in 6 well plates at a density of 5×10^4 cells/well. After 24 h cells were exposed to 200 µM PA-BSA conjugate and drug at indicated concentrations for 12 h. Cells were incubated with 5 µM of JC-1 dye (T3168, Invitrogen) for 40 min, followed by PBS washing for 30 min. The images were captured under a fluorescence microscope (Nikon ECLIPSE Ti- U, Japan)(Hu et al. 2019).

ELISA

For quantifying the inflammatory marker and BDNF in the brain hippocampus tissues were homogenized in TPER (Tissue Protein extraction reagent) buffer followed by sonication (20 pulses for 10 s), followed by centrifugation at 12,000 rpm for 5 min at 4^{O}C, the supernatants were collected, and total protein concentration was determined according to Micro BCA procedures. BDNF levels in tissue supernatants were assayed according to the supplier's protocol. Further plasma TNF-α and IL-4. Insulin was also quantified using the enzyme-linked immunosorbent assay (ELISA) kit) according to the manufacturer's protocol (Johnson et al. 2016).

Protein expression study

Western blot

Total proteins from cells were extracted using RIPA(radioimmunoprecipitation assay buffer)(cat no. R0278) respectively supplemented with a protease(cat no. p8340)-phosphatase(cat no. P-0044) inhibitor cocktail in 1:200. The lysed samples were sonicated using a probe sonicator at 20 pulses for 10 s and allowed for incubation on ice followed by centrifugation at 12,000 rpm for

20 min. The supernatant was collected, and protein estimation was carried out by using Bradford reagent (BIO-RAD) keeping BSA as standard. The hippocampus tissue was also homogenized in T-PER(Tissue Protein Extraction Reagent)(Cat no. 78510) buffer supplemented with protease and phosphates inhibitor cocktail in 1:200. The homogenized sample was further sonicated and allowed to centrifuge at 12000 g for 20 min. the supernatant was collected, and protein was estimated using Bradford (BIO-RAD). 20- 40 µg protein samples were resolved using 10,12,14% SDS-PAGE. Resolved proteins were transferred to the nitrocellulose membrane (BIORAD,1620112). The membrane corresponding to the desired protein was first blocked by incubating with 3% BSA followed by incubating them overnight at 4 °C with primary antibodies; NOS-II(SC7271), MHCII(ab180779), COX-II(SC7951), Arginase(ab60176), p-RIPK(53286S), p-MLKL(37333S), p-Tau (SC32275), p-RIPK3(91702S), Caspase-3(SC7272), Bax(SC7480), Bcl-2(SC7382), LC3B(127441 T), SQSTM(SC25575), DRP(SC-0.271583), synaptophysin (ab14692) On the 2nd day after washing with TBST, the membrane was incubated with corresponding HRP tagged anti-rabbit (SC2357) or anti-mouse (SC516102) or anti-goat(SC2354) secondary antibody for 2 h at room temperature. The chemiluminescence signal was captured using a Fusion-FX imager (Vilber Lourmat, Germany) to visualize the protein band and their relative intensities were quantified by densitometry using Image J software (version 1.48, NIH, USA).

Immunofluorescence (IF)

The Frozen brain section was taken out from -20 °C and kept for drying. Sections were given 3 washes of PBST followed by antigen retrieval in citrate buffer(Ph 6) in the microwave oven at 80 °C and washing in PBS. For mitotracker staining tissue sections were incubated with 10 µM mitotracker dye for 15–20 min in the dark Sections were blocked in 3% BSA in PBST for 1 h and then allowed to react with primary antibodies NeuN (MAB8377,1:100), IBA(32725S,1:50 and (17198S,1:200), P-RIPK(1:100), P-RIPK3(1:200), P-MLKL(1:200), SQSTM/p62(1:100), p-Tau(1:100), LAMP-1(1:100), LAMP-2(1:100), LC3B(1:200), CD16/32(SC,1:50), CD206(SC,1:50), TNFR(SC-8436) dilution for overnight. On the second day after retrieving the primary antibody sections were washed 3 times with PBS followed by incubation with Alexa fluor conjugated secondary antibodies at 4 µg/ml for 2–4 h (A11008, A11003, A21245, A11007). After incubation, tissue sections were washed thrice with PBS and mounted with Fluorosheild DAPI (Sigma Aldrich). Images were captured under 20x, 40x/1.30,63X oil under the confocal microscope (LEICA, DMi8) and the mean fluorescent intensity, Pearson coefficient, and Mender's coefficient were analyzed using Image-J software.

Immunocytochemistry(ICC)

Cells were grown on the poly-l lysin-coated coverslip. Cells were treated with indicated concertation drug and PA-BSA conjugate for 24 h. Later cells were washed with PBS, fixed with 4% PFA, and permeabilized with 0.1% triton x-100 in PBS. Further cells were washed, blocked with 3% BSA containing 0.3 M glycine for 1 h, and later incubated with appropriate primary antibodies P-RIPK(1:100), P-RIPK3(1:200), P-MLKL(1:200), p62(1:100), LAMP-2(1:100), Drp (SC271583,1:100), CD16/32(SC-20052), CD206(SC-376108) for overnight. On the second day after washing cells were incubated with secondary Alexa flour conjugated secondary antibody for 2 h. Finally, cells were washed thrice with PBS, and coverslips were mounted with Fluorosheild DAPI on the slide(Sigma Aldrich). Images were captured under 40x/1.30 oil under the confocal microscope (LEICA, DMi8) and the mean fluorescent intensity, Pearson coefficient, and Mender's coefficient were analyzed using Image-J software. For the Mitotracker colocalization study, after 24 h of treatment cells were incubated with a 5 µM Mito tracker for 30 min and were fixed with 4% PFA after brief PBS washing. The rest of the protocol follows the same steps as discussed above.

Quantitative real-time polymerase chain reaction (RT-qPCR) assay

RNA was isolated from the tissue using TRIzol reagent (Invitrogen). Total RNA was quantification and purity was checked in nanodrop (Thermo Fischer). The complementary DNA(cDNA) was synthesized using the TAKARA cDNA synthesis kit(Cat No, 6110 A).Further 1: 4 diluted cDNA was used for RT-PCR reaction using SYBR® Green Master Mix, ROX from Takara, and appropriate forward and reverse primers (Table S2). Quantitative reverse transcription–PCR was performed using (Instrument, Quant Studio 7 Pro Design with Analysis 2.6.0 Real-Time PCR System Applied Biosystem, Thermo Fischer). Relative mRNA expression changes were calculated from the comparative threshold cycle(Cq) value relative to mouse GAPDH.

Statistical significance

All measurements were carried out in triplicates, with a minimum of three independent experiments. Two-tailed unpaired Student's t-tests were used throughout this study

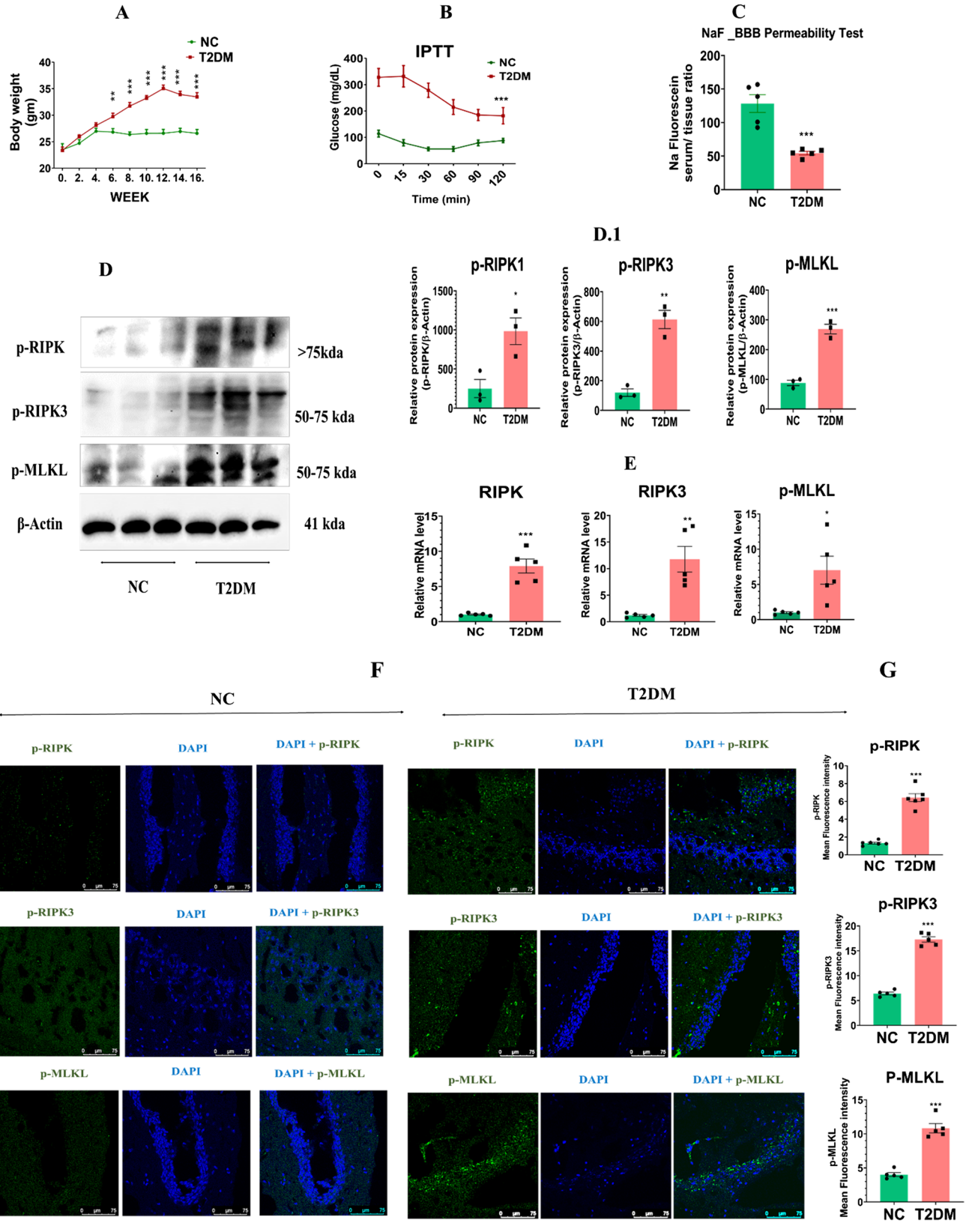
A
NC
T2DM
Body weight (gm)
WEEK
B
IPTT
Glucose (mg/dL)
Time (min)
C
NaF _BBB Permeability Test
Na Fluorescein serum/ tissue ratio
D
p-RIPK
p-RIPK3
p-MLKL
β-Actin
>75kda
50-75 kda
50-75 kda
41 kda
D.1
p-RIPK1
p-RIPK3
p-MLKL
Relative protein expression (p-RIPK/β-Actin)
Relative protein expression (p-RIPK3/β-Actin)
Relative protein expression (p-MLKL/β-Actin)
E
RIPK
RIPK3
p-MLKL
Relative mRNA level
F
NC
T2DM
p-RIPK
DAPI
DAPI + p-RIPK
p-RIPK3
DAPI + p-RIPK3
p-MLKL
DAPI + p-MLKL
G
p-RIPK
p-RIPK3
P-MLKL
Mean Fluorescence intensity

◂**Fig. 1** T2DM-associated metabolic syndrome led to the cognitive decrement, BBB damage, and activation of the necroptotic mechanism. **A-B**: Scatter plot of Body weight change($n=10$), IPTT($n=6$) between NC and T2DM. **C** Blood–Brain barrier Permeability Test, NaF tissue /serum ratio, NC($n=5$) vs. T2DM ($n=5$). **D**-D1 Western blot image of p-RIPK, p-RIPK3, p-MLKL of hippocampus tissue lysate and Scatter plot with bar graph showing densitometric analysis from NC ($n=3$) and diabetic group ($n=3$). **E**. Scatter plot with a bar graph showing relative mRNA level of RIPK, RIPK3, and MLKL hippocampus tissue. **F**. Immunofluorescence image showing relative fluorescence intensity of p-RIPK, p-RIPK3, and p-MLKL between NC and diabetic brain. **G**. Scatter plot with bar graph showing mean fluorescence intensity of p-RIPK, p-RIPK3, and p-MLKL between NC and diabetic brain. *Comparisons between groups were done by using Repeated 2-way ANOVA (Fig. 1B-C, E 1 F1-2, G1-2, I) and two-tailed unpaired t-test (Fig. 1D, G, H, I, J, L). p-value on figure indicates significance vs. NC group, *$p<0.05$, **$p<0.01$,***$p<0.001$*

to compare two distinct groups. To compare different groups at different time intervals; for instance, task learning and spatial acquisition were done from days 1 to 12, and two-way ANOVA, followed by the Bonferroni post hoc test was used. To compare between two groups, t-test and when more than two groups were compared, one-way Analysis of Variance. GraphPad Prism 8.2.2 software (GraphPad, San Diego, CA, USA) was used to assess all the significant differences. ANOVA, followed by the Bonferroni post hoc test was used. Data are expressed as mean with standard error mean (SEM), with a significant difference at $P<0.05$. * Indicates data compared with the normal control group and # for data compared with the diabetic group.

Result

T2DM-associated metabolic syndrome led to the cognitive decrement, DAM-like changes: Implication of p-RIPK, p-RIPK3, p-MLKL mediated necroptosis

T2DM metabolic syndrome is implicated in cognitive impairment and various investigators have used the (HFD + STZ) to induce experimental type T2DM in C57/BL/6 mice. However, to the best of us, our knowledge exact mechanism behind central dysfunction in terms of necroptosis has not been explored. Hence firstly we standardized the T2DM model in mice, and later cognitive decrement. The experimental protocol and timeline are performed by referring to the previously published reports as illustrated in (Fig. S.1A) (Kang et al. 2017; Lu et al. 2018; Park et al. 2020). We have noted weekly body weight changes for the entire 16 weeks before euthanizing the animals. A significant change in body weight starts appearing in the 6th week ($p=0.0224$) and continued till the 16th week in the HFD-fed group of animals (Fig. 1A) (Jeon et al. 2012). Hyperinsulinemia, hyperlipidemia, and hyperglycemia are important features of T2DM. Therefore, parameters like IPTT, PI, FBG, and lipid profile were evaluated. (HFD + STZ) group of animals has shown insulin tolerance (Fig. 1B). A significant increase in PI and FBG was observed in (HFD + STZ) group compared to the NPD-fed animals (Table S1). We used a battery of behavioral tests in one cohort of animals with a 2–3 day gap (Wolf et al. 2016). Mice of the HFD + STZ group have shown impaired spatial working memory ($p=0.0031$) in Y-maze (Fig. S1 B1-2), and episodic memory ($p=0.3186$) in NORT (Fig. S.1 C). They have also shown impaired task learning in terms of path length ($p=0.0065$), escape latency ($p=0.0088$) in visible and spatial learning; path length($p=0.0021$), escape latency($p<0.0001$) in hidden platform tests respectively (Fig. S.1 D1-2-E1-2), with impaired memory consolidation in terms of target crossing ($p=0.0118$), time spent in the target zone ($p=0.0087$), distance traveled in the target quadrant($p<0001$) (Fig. S.1 F, G, H) during probe trial in the MWM test. Further hippocampal-dependent aversive learning memory was also impaired as in terms of retention versus acquisition ($p=0.5698$) in the Step-through task/PAT (Fig. S.1 I). Consistent with available reports from various studies T2DM has led to both cortex and hippocampal-dependent learning and memory decrement. Previous investigators have emphasized the fact of T2DM causes BBB impairment(Takechi et al. 2017; Rom et al. 2019). Here to evaluate the same, we used NaF fluorescent dye, and the result was interpreted in terms of NaF in serum to brain tissue. Significantly higher amount of dye accumulated in the CNS compared to serum ($p=0.0003$) (Fig. 1 C). Although we could not rely on just the permeability test to infer about BBB health, and hence it needs further exploration. Meanwhile, in an already published study, Nec-1S has significantly diminished AD and insulin resistance-associated endothelial damage and further improved cognitive performance (Zou et al. 2020).

We have also performed the preliminary examination of liver, kidney, and pancreas structural changes. We performed H and E staining of a 5-micron thick paraffin section, and images were captured under 20-X magnification. The liver has shown a clear sign of fat globule (Fig. S2.A), the pancreas has shown diffuse islet cells (Fig. S2.B) and the kidney has shown glomerular changes (Fig. S.2- C), Further, we performed the western blot analysis for immune-related markers like NOS-II, Cox-II, MHC-II in the liver and kidney tissue. There was a significant increase in the expression of NOS-II ($p=0.0339$), COX-II ($p=0.0163$), and MHC-II ($p=0.0040$) in the liver and NOS-II ($p=0.0453$), COX-II ($p<0.0001$), and MHC-II ($p=0.0479$) in the kidney

of diabetic animals compared to NPD-fed animals (Fig. S2. A1-2, B1-2). The above proteins are also attributed to macrophage activation and hence we can say that the T2DM led to significant peripheral immune-associated perturbances. The previous finding has reported that macrophage activation in the periphery led to selective brain damage, however, we did not explore these aspects in the present study in detail.

Further, the relative abundance of p-RIPK1,p-RPK3, and p-MLKL protein was evaluated by WB analysis in hippocampus tissue.p-RIPK1 ($p = 0.0236$), p-RIPK3($p = 0.0018$), and p-MLKL($p = 0.0006$) were significantly higher in the diseased hippocampus tissue than in age-control normal animals (Fig. 1 D-D.1). The RT-PCR analysis has shown that the RIPK($p = 000,345$), RIPK3($p = 0.0011$), and MLKL($p = 0.0383$) mRNA levels were significantly increased in the hippocampus tissue at the mRNA level as well compared to normal control (Fig. 1 E). Further, the IF study has also revealed significantly increased expression patterns of p-RIPK($P < 0.0001$), RIPK3($p < 0.0001$), and p-MLKL($p < 0.0001$) in the hippocampus region compared to the diseased brain (Fig. 1 F-G).

As necrosomes formation is a prerequisite for executing p-MLKL-mediated necroptosis, we performed a colocalization study of p-RIPK3 and p-MLKL to validate the necrosome formation. There was a significant increase in the p-RIPK3 colocalization with p-MLKL($p = 0.0020$) as evaluated in terms of the Pearson coefficient in the diabetic brain compared to NPD-fed animals (Fig. 2 A-A1). A similar necrosome was also reported in the brain section of postmortem AD and another disease model (Rodriguez et al. 2015; Caccamo et al. 2017; Weber et al. 2018).

To know the relative abundance of p-RIPK, p-RIPK3, and p-MLKL in neurons we performed their colocalization Study with NeuN, a neuronal marker. All three colocalize with neurons without any significant difference ($p > 0.05$) (Fig. 2 C1-C3 and D1). As CNS is enriched with both Neuron-glia, the two very different types of cells. They work in coordination with normal brain functioning and respond differently under stress(Preeti et al. 2021). Therefore, we performed p-MLKL colocalization with IBA (Microglia marker). p-MLKL colocalizes with both neurons and microglia but it was significantly higher with neurons compared to IBA ($p = 0.0019$) (Fig. 2 C3-4 and D2).

The T2DM-mediated metabolic stress also led to central inflammation by activation of microglia. To check their activation, we performed the IF study of microglia by labeling them with IBA. The mean intensity was measured using Image J software. A significant increase in the mean intensity for IBA($p < 0.0001$) was observed in hippocampus region (Fig. 2-B-B1). Microglia especially have shown longer branches and swollen cyton in the diseased brain (Fig S-3). (From here onwards we will use the DAM term for microglia in the diseased brain).

Palmitate-mediated lipotoxicity leads to increase in necroptosis marker in Neuro2A cells: Comparative effect of Necrostatin and GSK-872 on necroptosis

The p-RIPK, p-RIPK3, and p-MLKL are the 3 main executioners of necroptosis, and hence to inhibit that we could use either of 3 well-known small molecules i.e., Nec-1S as RIPK1 inhibitor(Jantas et al. 2020), GSK-872 as RIPK3 inhibitor (Hou et al. 2019) and necrosulfonamide (NSA) as MLKL inhibitor(Sun et al. 2012). All 3 have been used previously in different disease models and mechanistic studies. As we were trying to see the MLKL modulation by RIPK, RIPK3, and p-MLKL aftereffects, NSA was not considered in the comparative study. p-MLKL majorly colocalized with neurons and microglia. We will be using N2A and BV2 cells (which will be discussed later) for further studies. N2A cells are mouse neuroblastoma cell lines and are being used for various neurodegeneration and neurotoxicity studies(AU et al. 2017; Jauhari et al. 2020). We used different concentrations of PA-BSA conjugate and tried to find out the one which can induce the necroptotic protein expression by western blot, besides performing the MTT-based cell viability study. PA-BSA conjugate has led to significant death at 400 and more in the MTT test (supplementary file 3a.). The western blot study has led to conclude that 200 µM PA-BSA (hereafter we will use P-200) is the optimum for further mechanistic study as P-200 and P-300 significantly increased the expression of p-RIPK, p-RIPK3,p-MLKL in N2A cells (Fig. 3A & A1-A3). Cell viability test of Nec-1S and GSK-872 (alone) and (in the combination with PA-BSA) was performed (supplementary files 3b,c, and 4a,b). Based on the reported dose of Nec-1S, GSK-872, and the MTT test 2 different concentrations of Nec-1S (25 & 50 µM) and GSK-872(5 and 10 µM) were used for further study. Western blot study has shown that both concentrations of Nec-1 s (N-25, N-50) have significantly decreased the p-RIPK ($p < 0.0001$) and p-MLKL($p < 0.0001$) expression (Fig. 3-B, B1-B2). GSK-872 at doses of (G10, G-5) have significantly ($p < 0.0005$) decreased p-RIPK3 expression but there was no change in p-MLKL expression ($p = 0.1926$) (Fig. 3C and C1-C2). Further, we evaluated the N50 and G10 effect on p-RIPK3 and p-MLKL colocalization in N2A cells under lipotoxic stress. P200 significantly increased the p-MLKL mean intensity ($p < 0.0001$) and its colocalization with p-RIPK3 as evidenced by the Pearson coefficient analysis ($p < 0.0001$) compared to vehicle control (BSA treated cells) whereas both have decreased the p-MLKL mean intensity N50($p < 0.0001$) and G-10($p = 0.0022$), and colocalization, N50 ($p < 0.0014$) and G-10 ($p < 0.0075$),

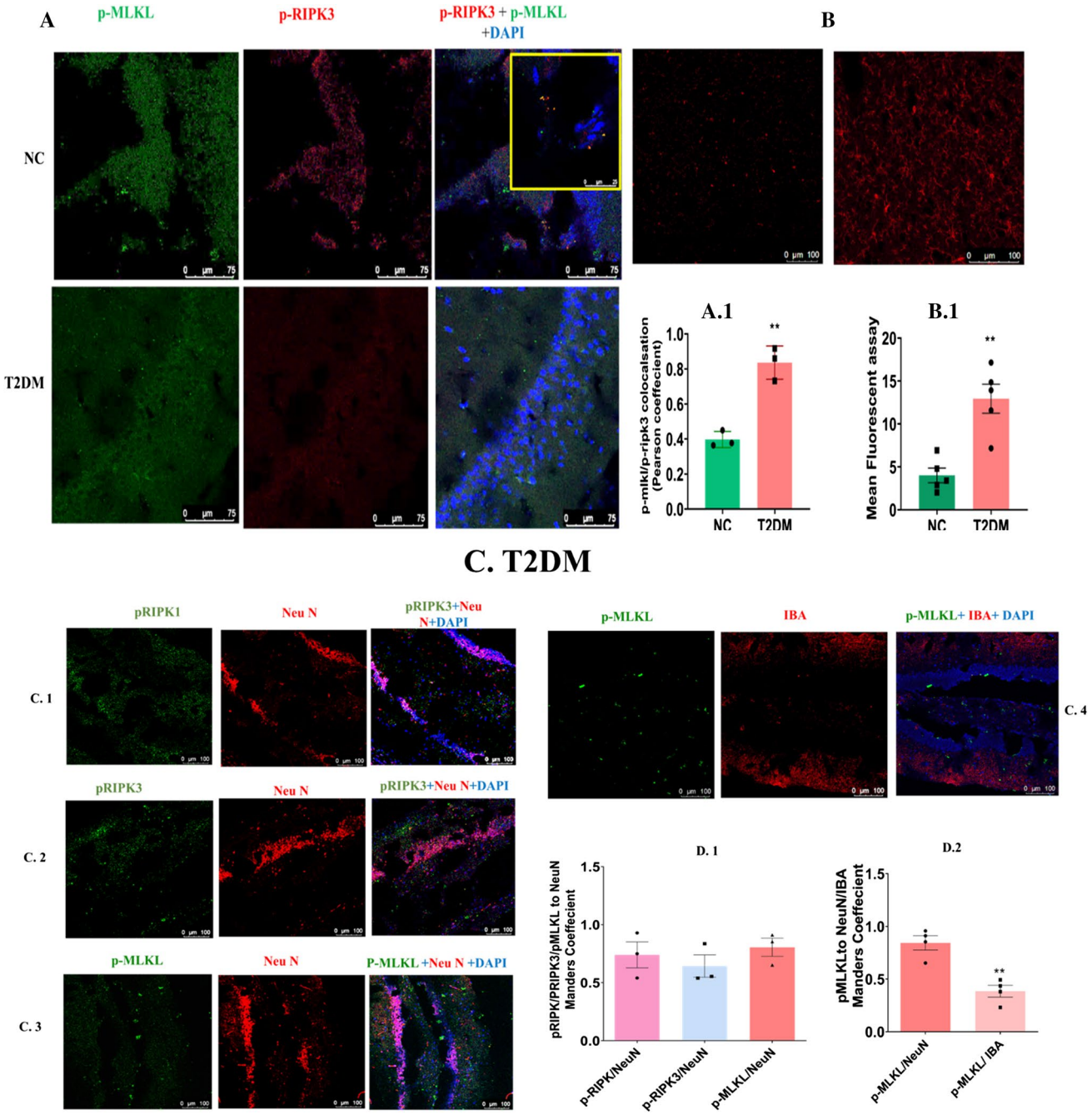

Fig. 2 Necroptosis involves necrosome formation, p-RIPK, p-RIPK3, and p-MLKL relative colocalization to neuron, microglia, and microglia activation. **A** Colocalization of p-RIPK3 and p-MLKL in the brain under (40×and magnified area (top right) NC (lower panel), T2DM (upper panel), left (p-MLKL), Middle (p-RIPK3) right (Merge Image). **A2** Scatter plot with a bar graph showing Pearson coefficient of p-RIPK3 and p-MLKL colocalisation. NC vs. T2DM ($n=3$). **B-B1** Immunofluorescence image of microglia changes in hippocampus region (20×magnification) and quantification of fluorescent intensity of NC (left panel) vs.T2DM (right panel) ($n=3$). **C, C1-3** Immunofluorescence image showing colocalization of p-RIPK, p-RIPK3, and p-MLKL to NeuN in the diabetic brain under (20x) (p-MLKL lower panel), p-RIPK3 (middle panel), p-RIPK (upper panel), Left panel (p-MLKL, RIPK3, RIPK), Middle panel (Neu-N) panel (Merge Image). **C4** Immunofluorescence image showing colocalization of p-MLKL to IBA in the diabetic brain under (20x) right (Merge Image). **D1** Scatter plot with bar graph showing the relative colocalisation of p-MLKL, p-RIPK3, p-RIPK to NeuN as Mander's coefficient. **D2** Scatter plot with bar graph showing the relative overlap of p-MLKL to NeuN/IBA as Mander's coefficient. *Comparisons between groups were done by using one-way ANOVA followed by "Bonferroni's multiple comparison post-hoc test". p-value on figure indicates significance vs. p-MLKL/NeuN vs *$p<0.05$, **$p<0.01$ for figure D1*

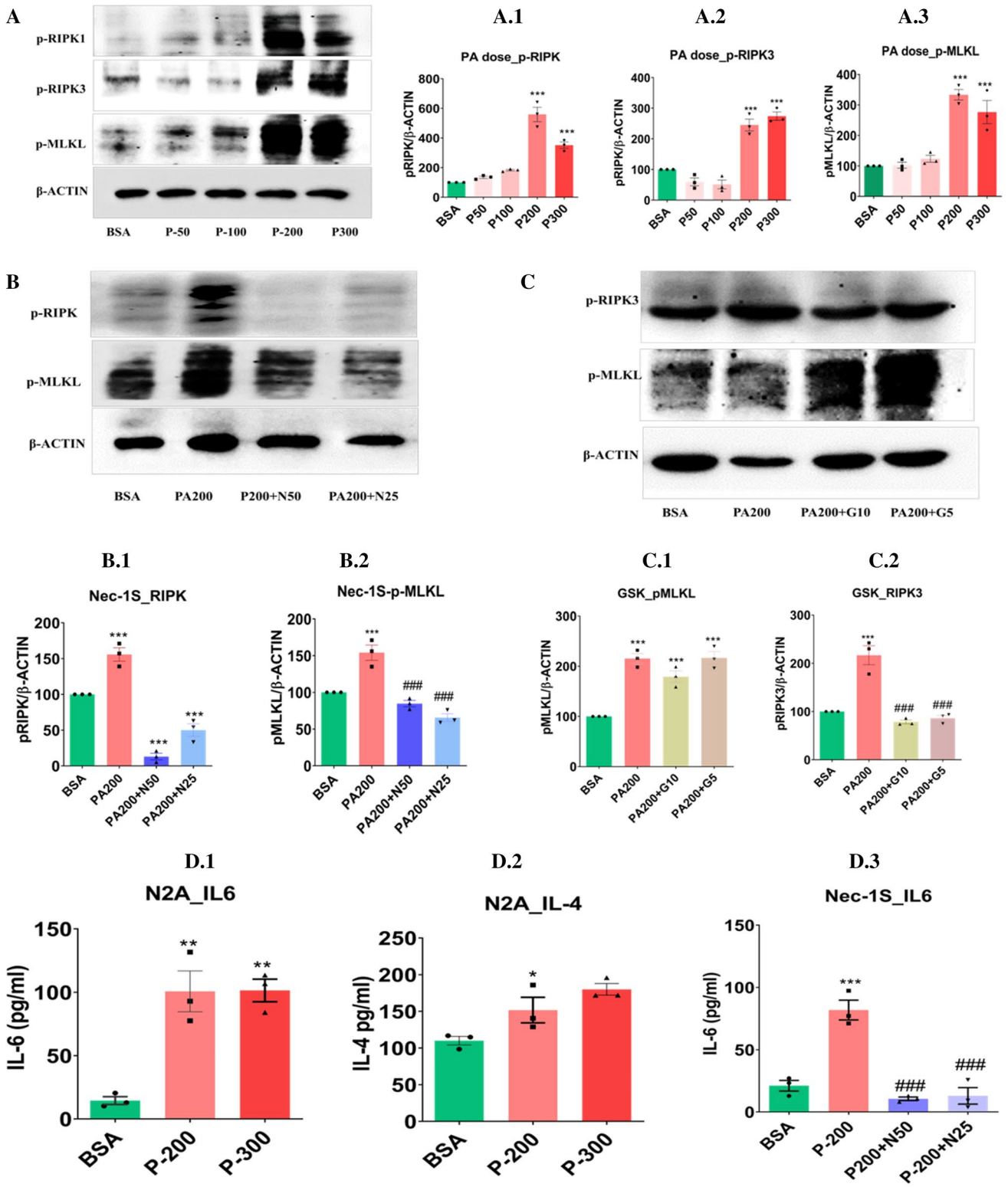

although N50 has more inhibitory effect compared to G10 (Fig. 4 A, A1-2). Further, ELISA for IL6 and IL-4 was performed in cell supernatant for P-200 and P-300 doses where PA-BSA conjugate led to an increase in IL-6 ($p < 0.001$) at both doses however there was a slight increase in IL-4 ($p = 0.0156$) in P-300 (Fig. 3 D1-2).Further pretreatment

◂**Fig. 3** Palmitate-mediated lipotoxicity increases the necroptosis marker in Neuro2A cells: Comparative effect of Necrostatin and GSK-872 on necroptosis. **2A, A1-A3** Palmitate dose standardization: Western blot image of p-RIPK, p-RIPK3, p-MLKL from N2A cell and their densitometric analysis. P-50, P-100, P-200, P-300 vs. BSA group (vehicle). **2B, B1-B2** Western blot analysis for the comparative effect of two different doses of Nec-1S, i.e., N50 and N25 on p-RIPK, p-MLKL expression their densitometric analysis showing the relative percentage density. **2C, C1-C2** Western blot analysis for the comparative effect of two different doses of GSK-872, i.e., G10 and G5 on p-RIPK3, p-MLKL expression and their densitometric analysis showing the relative percentage density. **2D1-2** IL- 6 and IL-4 levels in cell supernatant. **2 D3** Nec-1S effect on IL-6 secretion. *Comparisons between groups were done by using one-way ANOVA followed "Bonferroni's multiple comparison post-hoc test". p-value on figure indicates significance *p < 0.05, **p < 0.01,***p < 0.001 vs. BSA and # p < 0.05, ##p < 0.01, ### p < 0.001 vs. P-200*

of N-50 & N-25 both have significantly decreased the IL-6 production ($p = 0.0001$)(Fig. 3 D3). The IL-6 and IL-4 have their modulatory effect on microglia which will be discussed in the microglia section.

Nec-1S treatment improved cognitive performance in T2DM mice: Decrease in degenerative neuron, amyloid oligomer, and phospho-Tau deposits

Further, we selected Nec-1S for animal study to evaluate its CNS protectant effect. Nec-1S was chosen based on the discussed result and previously reported studies. The timeline of the study is illustrated in Fig. Nec-1S has not only inhibited the necroptosis mediator but also decreased the amyloid deposit, and in one of the recent studies, Nec-1S has elevated the BDNF level (Yin et al. 2021). In the present study, after 16th weeks animals under (HFD + STZ) were further divided into groups, one continued on HFD with vehicle administration (2.5% DMSO in saline), and another received Nec-1S. Nec-1S did not bring any change in body weight ($p > 0.05$), IPTT, and OGTT profiles (Fig. 5 B-D). Nec-1S also did not bring any change in FBG and TC levels ($p > 0.05$). Meanwhile, a decrease in the blood sugar level and glucose tolerance was observed in addition

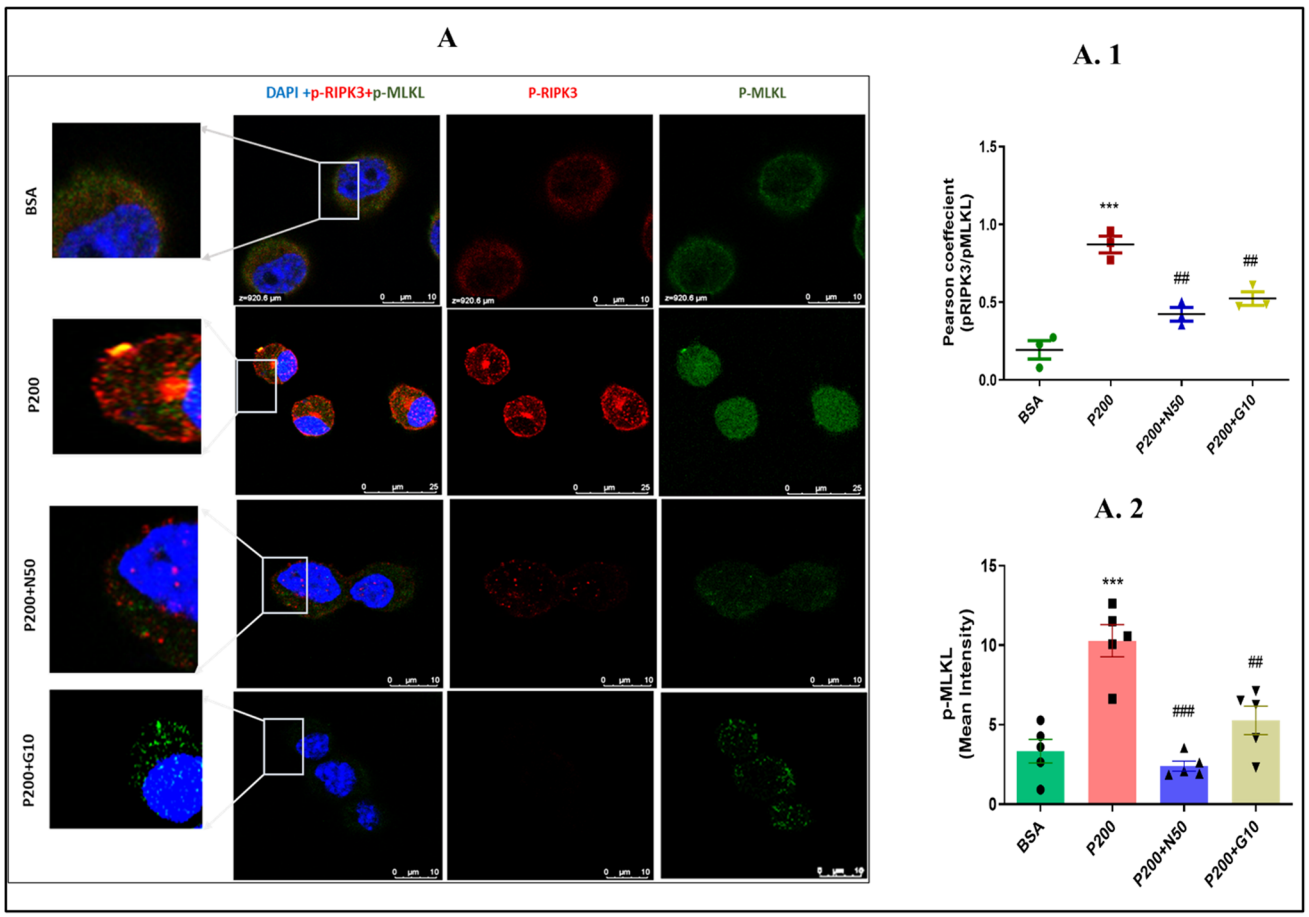

Fig. 4 Palmitate-mediated lipotoxicity effect on necrosome formation Comparative effect of Necrostatin and GSK-872 on necroptosis. **2D** Immunofluorescence image showing colocalization of p-RIPK3 and p-MLKL in N2A Cell under (40× and magnified area (left panel) BSA treated (upper panel), P-200(2nd panel), P-200 + N50 NC (3rd panel), P-200 + G10 (4.th panel) right (p-MLKL), Middle (p-RIPK3) Left (Merge Image). **2D.1** Scatter plot of Pearson coefficient a measure of colocalization efficiency ($n = 3$). **2D.2** Scatter plot with bar graph showing the mean intensity of p-MLKL between different groups ($n = 5$)

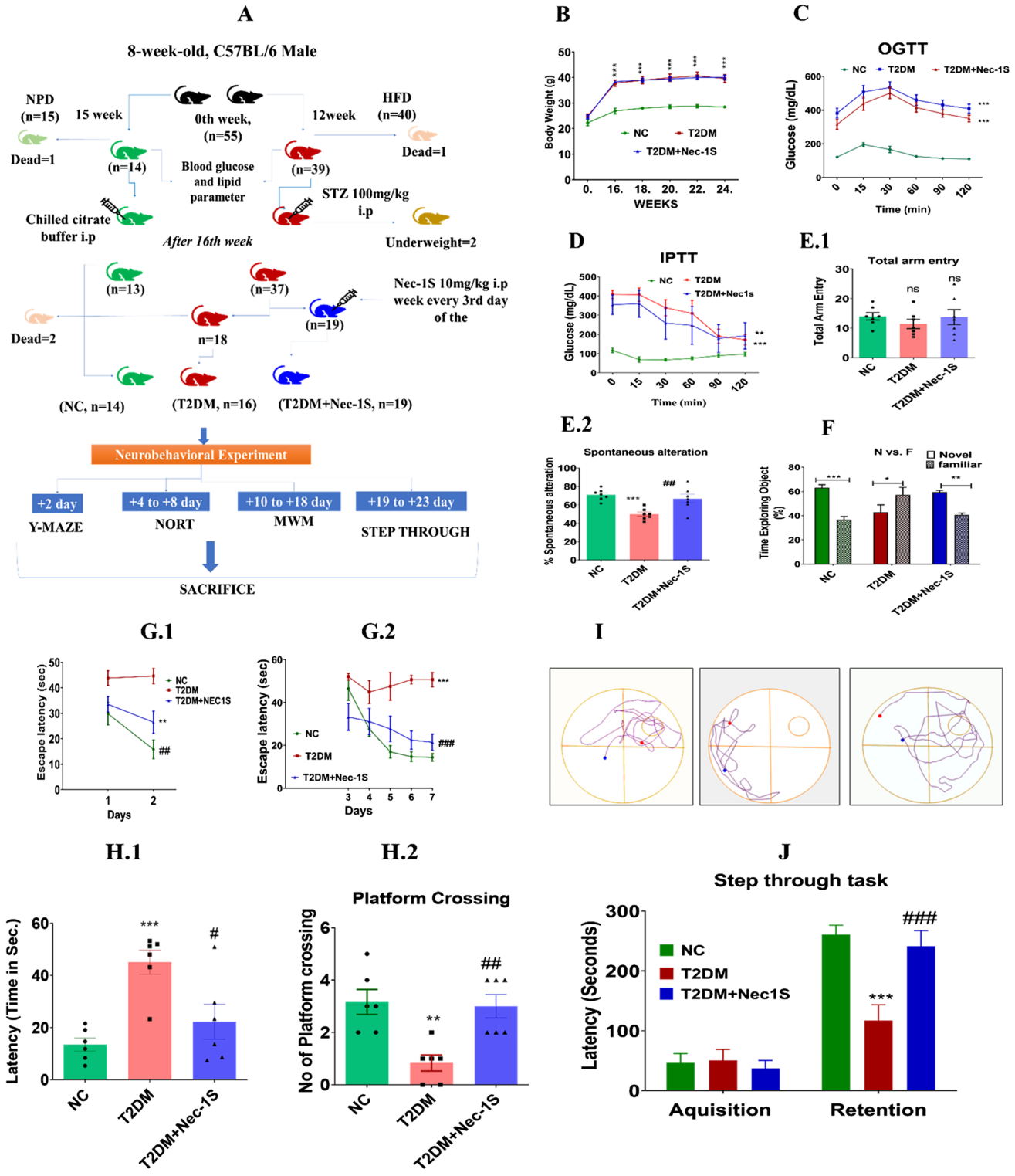

to a significant decrease in the TG level ($p = 0.002$) compared to diabetics (Table 2). The above finding is also in accordance with the previous finding where Nec-1S has improved hepatic insulin sensitivity and also modulated the lipid profile(Xu et al. 2019). Nec-1S has significantly alleviated the peripheral inflammatory cytokine such as TNF-α ($p < 0.0001$), and IL-6 ($p = 0.0099$) levels whereas increased the IL-4 ($p = 0.0131$), one of the antiinflammatory cytokine levels in plasma compared to diabetic group (Table2). Further, we evaluated the effect of Nec-1S treatment on cognitive performance. Treated animals have shown slight improvement in spatial working memory in the Y-maze

◂**Fig. 5** Nec-1S treatment improved cognitive performance in T2DM mice. **A.** Study design and timeline for Nec-1S dosing. **B**. Body weight change from the 16-24th week ($n=6$). **C.** OGTT between, NC($n=6$), T2DM($n=7$) and T2DM + NEC-1S($n=6$) group. **D.** IPTT between, NC, T2DM, and T2DM + Nec-1S ($n=5$). **E.1–2** Scatter plot with bar graph analysis of Y maze test NC ($n=7$) T2DM ($n=7$) and T2DM + Nec-1S ($n=7$). **F.** Bar graph of NORT test between NC($n=7$), T2DM($n=9$), and T2DM + Nec-1S ($n=9$). **G.1** Day 1–2 Task learning during visible platform test NC($n=6$), T2DM($n=6$), and T2DM + Nec-1S ($n=6$). **G.2** Day 3-7.th spatial learning in hidden platform in term of escape latency NC($n=6$),T2DM($n=6$) and T2DM + Nec-1S ($n=6$). **H.1–2** Day 8 probe trial escape latency, target crossing NC($n=6$), T2DM($n=6$), and T2DM + Nec-1S ($n=6$). **I.** Track the plot from the day of the probe trial. Step through/Passive Avoidance test NC ($n=6$), T2DM ($n=6$) and T2DM + Nec-1S ($n=6$). *For 3.1 B, G1-2, Comparisons between groups were done by using Two -way ANOVA. p-value on figure indicates significance *p < 0.05, **p < 0.001,***p < 0.0001 vs. NC and # p < 0.05, ##p < 0.001, ### p < 0.0001 vs. T2DM. Comparisons between groups were done by using one-way ANOVA followed by "Bonferroni's multiple comparison post-hoc test". p-value on figure indicates significance vs. NC *p < 0.05, **p < 0.01,***p < 0.001, and, vs. T2DM # p < 0.05, ##p < 0.01, ### p < 0.001*

test($p=0.0006$)(Fig. 5E1-2) with significant improvement in exploratory behavior or episodic memory ($P=0.0055$) in the NORT test (Fig. 5F). Nec-1S treated animals have shown improved task($p=0.0040$) (Fig. 5G1) spatial learning and memory acquisition($p<0.0001$) (Fig. 5G2) memory consolidation in terms of escape latency($P=0.0153$),and platform crossing($p=0.0068$) (Fig. 5,H1-2) in MWM test. The other behavior which we noticed was that diabetic animals have shown significant thigmotaxic behavior data not analyzed. A significant improvement in hippocampal-dependent aversive learning memory was also observed in the Step-Through task ($p<0.0001$) (Fig. 5J).

Further FJ-C staining was performed to evaluate neurodegenerative changes. Nec-1S treatment has significantly decreased ($p=0.0091$) the FJ-C positive neuron compared to the diabetic brain (Fig. 6 A-A1). Metabolic stress like T2DM-associated central changes also shows phosphorylated Tau and Amyloid oligomer deposits. Hence, we performed a phospho-Tau IF and western blot study. The diabetic brain has shown a significant increase of p-Tau ($p=0.0010$) in the hippocampus which was found to be diminished in the Nec-1S-treated brain ($p=0.0018$). Nec-1S treatment has also shown a decrease in p-Tau blot density in the hippocampus ($p=00{,}216$ compared to the diabetic brain. The RT-PCR study has revealed an increased mRNA level($p=0.0031$) compared to NC; however, no significant difference was observed in the treated brain($p=0.0591$). To check for synaptic profile, we assessed the synaptophysin expression pattern by western blot. A significant decrease in synaptophysin expression ($p=0.0048$) was observed in the diabetic brain. Whereas Nec-1S treated group has shown improved synaptic protein expression ($p=0.0406$) (Fig. 6 C and C1-2).

We have performed Thioflavin-S staining, which gives incite only about amyloid oligomer and not mature plaque. The diabetic brain has shown a significant increase in oligomer deposit ($p=0.0013$), and here also Nec-1S has decreased the incidence of oligomer deposit ($p=0.0077$)

Table 2 Plasma biochemical parameter (study 2)

Plasma biochemical parameter			
Parameters	NC	T2DM	T2DM + Nec-1S
FBG	120.6 ± 11.30 mg/dl ($n=6$)	350.3 ± 27.31 mg/dl***($n=6$)	300.8 ± 37.06 mg/dl$^{\#\#\#}$ ($n=6$)
TC	73.38 ± 3.20 mg/dl ($n=6$)	208.7 ± 28.47 mg/dl**($n=6$)	198.4 ± 23.36 mg/dl$^{\#\#}$ ($n=6$)
TG	36.44 ± 1.37 mg/dl ($n=6$)	55.27 ± 4.32 mg/dl**($n=6$)	40.18 ± 1.59 mg/dl $^{\#\#}$ ($n=6$)
HDL	69.66 ± 5.97 ($n=6$)	61.06 ± 7.46 mg/dl ns ($n=6$)	68.61 ± 7.01 ns ($n=6$)
Plasma cytokines			
TNF-α	77.96 ± 10.45 pg/ml ($n=6$)	292.9 ± 57.60 pg/ml***($n=6$)	80.19 ± 13.09 pg/ml $^{\#\#\#}$($n=6$)
IL-4	778.00 ± 67.68 pg/ml ($n=6$)	365.2 ± 72.52 pg/ml*($n=6$)	715.6 ± 80.98 pg/ml$^{\#\#}$($n=6$)
IL-6	7.9 ± 1.47 ($n=6$)	38.12 ± 5.98***($n=6$)	18.74 ± 2.879$^{\#\#}$ ($n=6$)
Hippocampus tissue			
TNF-α	140 ± 7.2 pg/mg tissue ($n=6$)	310 ± 18.49 ***pg/mg tissue ($n=6$)	206.1 ± 24.52$^{\#\#}$ pg/mg tissue ($n=6$)
BDNF	358.6 ± 16.00 pg/mg tissue ($n=3$)	108.1 ± 6.95*** pg/mg tissue ($n=3$)	229.8 ± 22.11$^{\#\#}$ pg/mg tissue ($n=3$)

FBG: Fasting Blood Glucose, TC: Total Cholesterol, TG, triglycerides, HDL: High-density lipoprotein, IL-4: interleukin-4, IL-6:interleukin-6; TC, total cholesterol; TG, triglycerides; TNFα, tumor necrosis factor-α. BDNF (Brain-derived neurotrophic factor). All parameters were measured at the end of the study Plasma markers were measured following a 4 h fast., One-way ANOVA followed by Tukey's multiple comparisons test)

Comparisons between groups were done by using one-way ANOVA followed "Bonferroni's multiple comparison post-hoc test"

*p-value on figure indicates significance *p < 0.05, **p < 0.01,***p < 0.001 vs. NC and,*

$^{\#}$ p < 0.05, ##p < 0.01, ### p < 0.0001 vs. T2DM

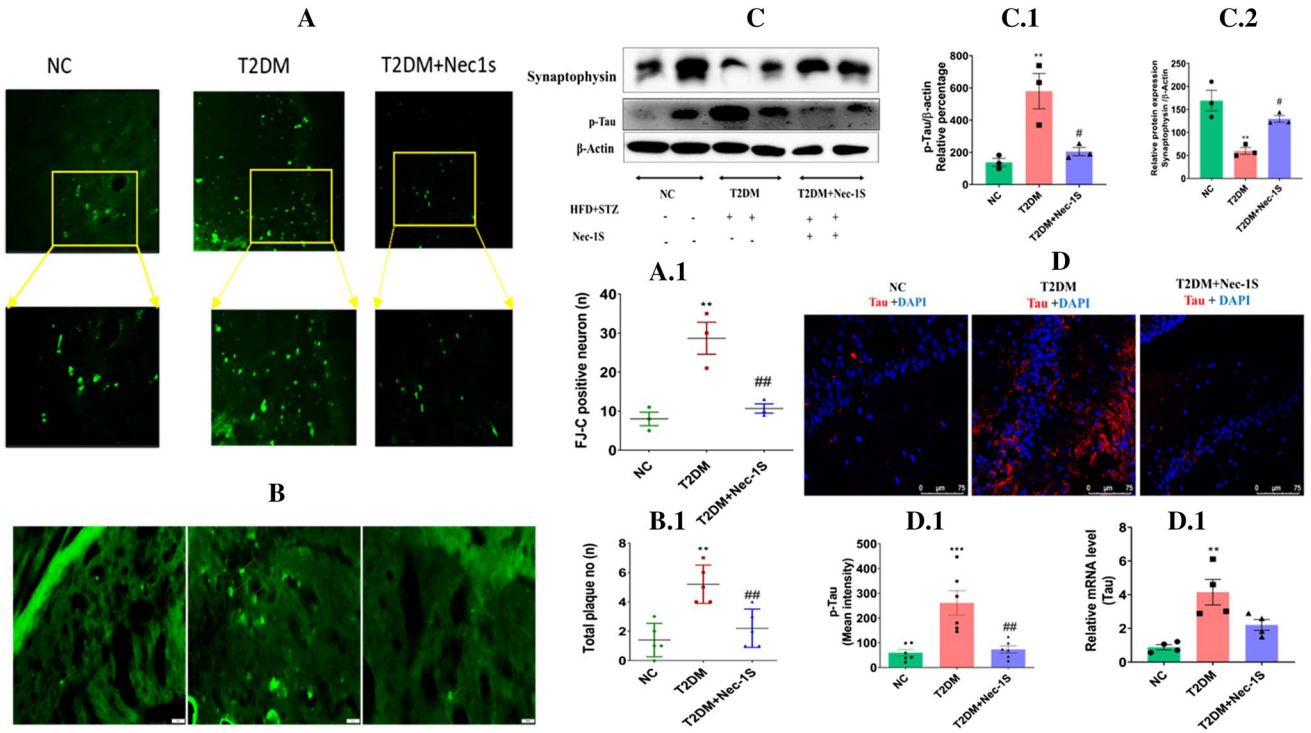

Fig. 6 Nec-1S ameliorates degenerative neuron, amyloid oligomer, and phospho-Tau *deposits.* **A-A.1** Fluorescence image showing the FJ-C positive neuron (20× and magnified area (left panel) NC (upper panel), T2DM (2nd panel), T2DM + Nec-1S (3rd panel). and scatter plot representing the relative difference in FJ-C neurons. **B-B.1** Fluorescence image showing the amyloid oligomer deposit in the brain (20× magnification) NC (upper panel), T2DM (2nd panel), T2DM + Nec-1S (3rd panel) and scatter plot representing the relative difference in plaque no. **C-C1-2** Western blot image of **s**ynaptophysin**,** phospho-Tau deposit ($n=3$) in the hippocampus and scatter plot with bar graph represents densitometric analysis showing the relative percentage density between different groups. **D-D.1** Fluorescence image showing the phospho-Tau deposit in hippocampus (40× magnification) NC (upper panel), T2DM (2nd panel), T2DM + Nec-1S (3rd panel). scatter plot with a bar graph showing the mean intensity of phospho-Tau($n=6$). **D.2** Relative mRNA of Tau change between different groups ($n=4$). *Comparisons between groups were done by using one-way ANOVA followed by "Bonferroni's multiple comparison post-hoc test". p-value on figure indicates significance* $*p<0.05$, $**p<0.01$, $***p<0.001$ *vs. NC and,* # $p<0.05$, ## $p<0.001$, ### $p<0.001$ *vs. T2DM*

(Fig. 6 B-B1). However, the author feels the need for a detailed study regarding oligomer deposits. Additionally, we did not decipher timeline changes as to when the deposits might have started and which of the event i.e., phospho-Tau deposits or amyloid deposits are indispensable for each other and correlated to cognition perse.

Nec-1S alleviated the expression of necroptosis and apoptotic protein

To understand the underlying mechanism or the secondary effect of Nec-1S, we have carried out the western-blot study for p-RIPK, p-RIPK3, and p-MLKL. Nec-1S has significantly alleviated the expression of all the key proteins in the hippocampus: p-RIPK($p=0.0039$),p-RIPK3($p<0.0001$), p-MLKL(0.0035)(Fig. 7A-B) involved in necroptosis which was elevated in the diabetic brain. Further, we have also explored the effect of Nec-1S on apoptotic proteins like Bax, Caspase-3, and cleaved caspase 3. The diabetic brain has shown a significant increase in apoptotic proteins such as BAX($p<0.000$), caspase3($p<0.0197$), and cleaved caspase3($p<0.0015$) in the hippocampus tissue of the brain. Further, Nec-1S treatment has decreased the expression of apoptotic protein Bax ($p=0.0002$), caspase-3 ($p=0.0285$), and cleaved caspase3 ($p<0.0046$) expression in the hippocampus (Fig. 7 D & D1). The anti-apoptotic effect of Nec-1S could be related to its indirect mitoprotective potential (which will be discussed in detail in the next section). The RIPK1 has previously been reported to have the regulating delayed apoptotic event also and hence this could also be the rationale for having the antiapoptotic effect of Nec-1S (Remijsen et al. 2014; Zhang et al. 2019). We also performed the IF study to evaluate the relative expression pattern of p-MLKL in the hippocampus in both diseased and treated brain sections. The Nec-1S treatment has significantly decreased the mean fluorescent intensity of p-MLKL in the hippocampus ($p=0.0038$) compared to the diseased brain (Fig. 7 C & C1).

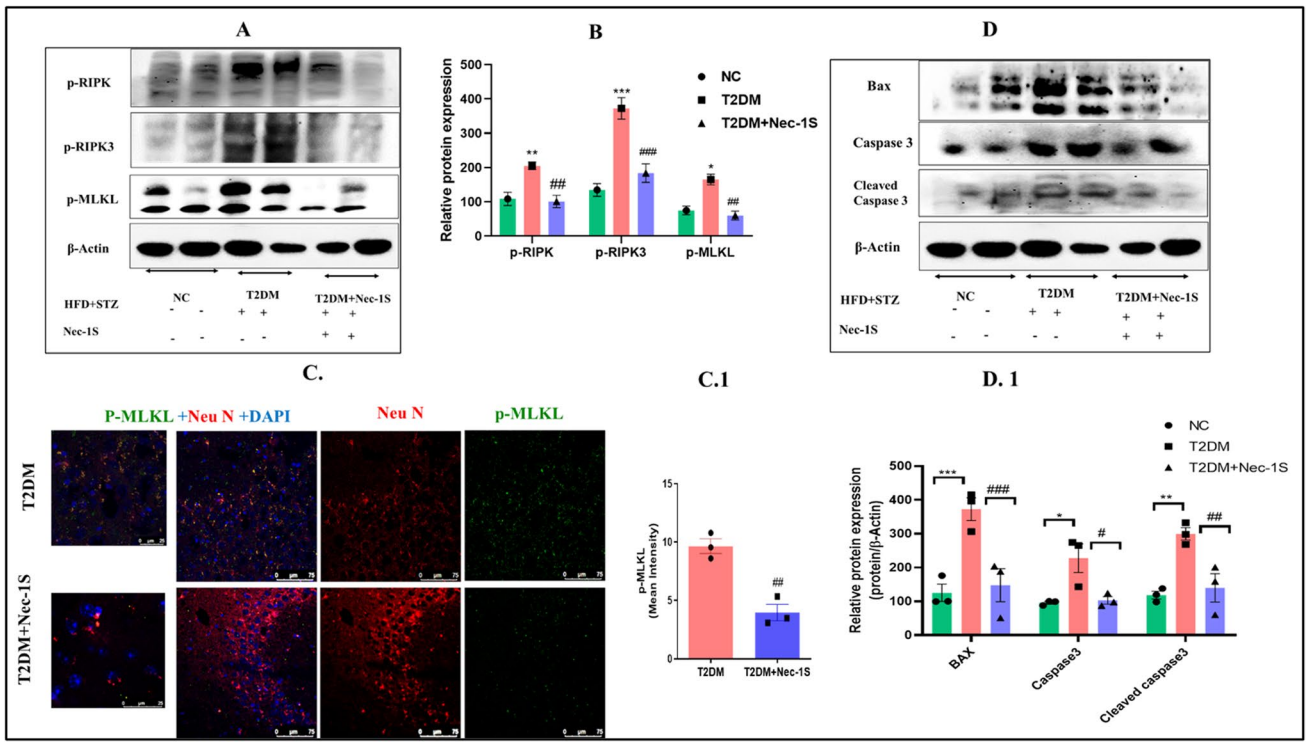

Fig. 7 Nec-1S alleviated the expression of necroptosis and apoptotic protein in the hippocampus tissue. **A-B** Western blot image of necroptosis mediator p-RIPK, p-RIPK3,and p-MLKL in the hippocampus and their densitometric analysis, the scatter plot with bar graph is showing relative percentage of blot density between T2DM vs. T2DM + Nec-1S ($n = 3$). **C-C1** Immunofluorescence image showing colocalization of p-MLKL to NeuN in the brain of T2DM and T2DM + Nec-1S under 40× magnification, the magnified version in the left panel. p-MLKL (Right panel), Neu-N (Middle panel) Merge Image (left panel). Scatter plot with bar graph showing the mean fluorescent intensity of p-MLKL in T2DM vs. T2DM + Nec-1S. *(β-actin is same for Fig A and D as the corresponding proteins western blot were carried out on single run). Comparisons between groups were done by using one-way ANOVA followed by "Bonferroni's multiple comparison post-hoc test". p-value on figure indicates significance *$p < 0.05$, **$p < 0.01$,***$p < 0.001$ vs. NC and, # $p < 0.05$, ##$p < 0.001$, ### $p < 0.001$ vs. T2DM*

Necroptosis is intricately involved in mitochondrial dysfunction and autophago-lysosomal clearance mechanism: Exploring pRIPK3/ pMLKL aftereffects

As we have discussed while introducing the topic that, p-MLKL can fuse and damage the other subcellular organelle like mitochondria and lysosomes. However, there is a lack of detailed research background in support of this idea. The present study also could not explore much here and has only managed to explore a few of them.

We have discussed Bax, an important mitochondrial resident protein, expression patterns. Previously, DRP, MFN, and FIS-mediated mitochondrial fission/fusion imbalance have been associated with metabolic brain disease (Hu et al. 2017; Zuo et al. 2019) and neurodegenerative disorder (Joshi et al. 2018; Park et al. 2021; Preeti et al. 2021). Later has been correlated to the changes in mitochondrial membrane potential changes MMP (Ψm). Exposure to PA-BSA conjugate has significantly diminished the mitochondrial membrane potential (MMP/Ψm) in N2A cells compared to BSA-treated cells ($P = 0.0018$). Moreover, pretreatment with both the small molecule Nec-1S and GSK-872 at N-50($p = 0.0184$) and G-10 ($p = 0.0377$) dose, has maintained the MMP (Ψm) indicated as a red/ green or JC-1 aggregate to monomer mean intensity ratio (Fig. 9 A-A1).To explore p-MLKL insertion to mitochondria, we used a mitotracker dye to monitor the mitochondrial-rich region in cells and performed ICC. P-200 has significantly increased the percentage overlap of p-MLKL to mitotracker represented in terms of Mander's coefficient ($p = 0.0018$) compared to BSA-treated cells. Both Nec-1S ($p = 0.0063$) 0.0001), and G-10 ($p = 0.0232$) have decreased the percentage overlap with mitotracker. Nec-1S has brought more significant changes in comparison to G10 in preventing p-MLKL-mediated mitochondrial dysfunction (Fig. 9 C-C1). The p-RIPK3 kinase activity phosphorylates MLKL and is also responsible for Drp phosphorylation via PGAM5, a mitochondrial phosphatase (Zhou et al. n.d.). Drp contributes to mitochondrial fragmentation, ultimately disturbing their homeostasis.

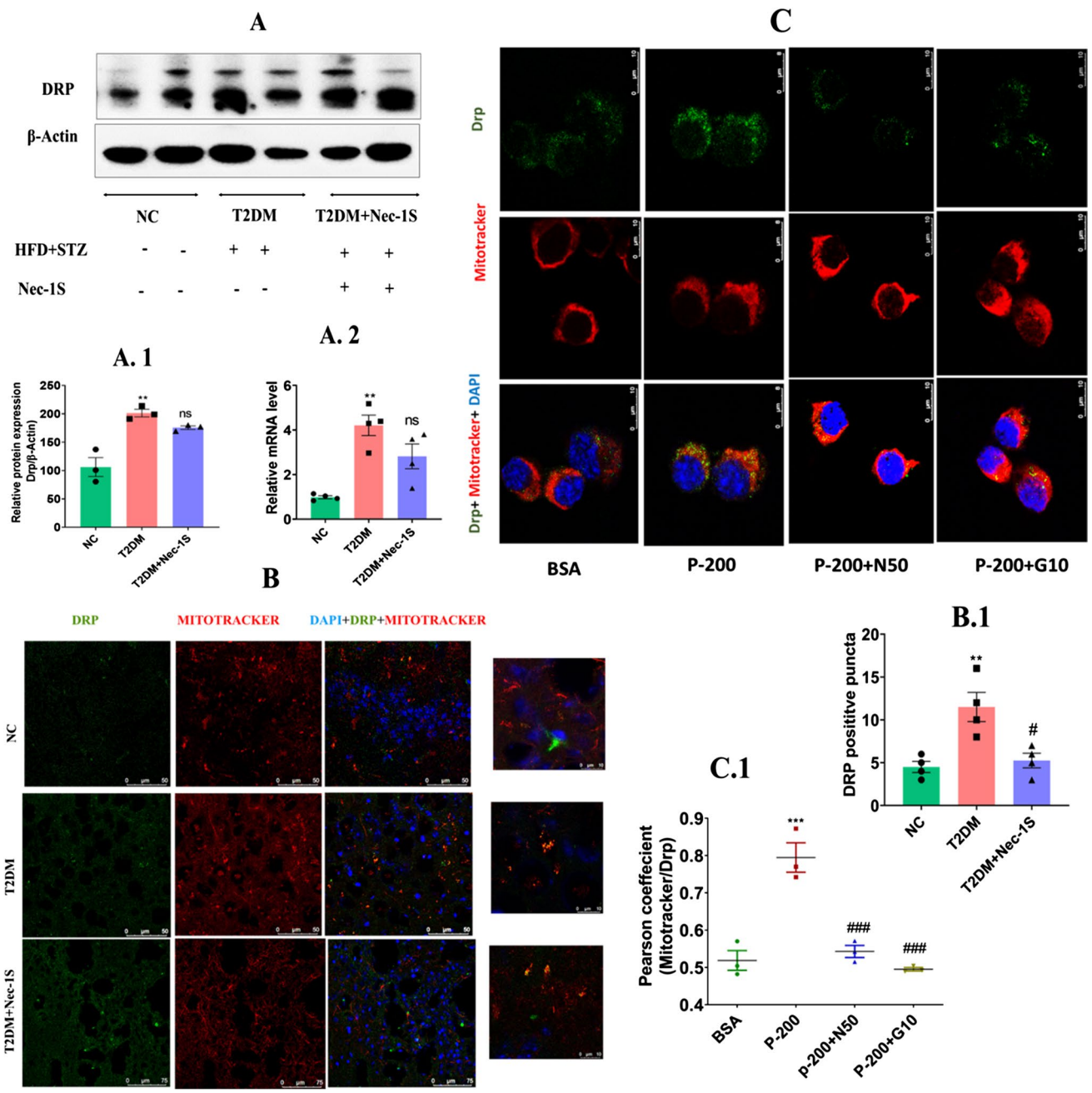

Fig. 8 Effect of Nec-1S and GSK-872 on p-RIPK3 and Drp localization with mitochondria in tissue and cell. **A-A1** Western blot of Drp and scatter plot with bar graph showing the densitometric analysis of DRP expression in hippocampus tissue between different groups ($n=3$) *(β-actin is same as of Fig. 3.3 A and D as the corresponding proteins western blot were carried out on single run).* **A2.** Relative mRNA level of DRP between different group. **B-B.1** Immunofluorescence image showing the colocalization of Drp with mitochondria in the hippocampus region of mice brain section under 63×magnification. Left panel (Drp), Middle panel (Mitotracker), right panel (merge image). Scatter plot with bar graph showing the relative overlap of Drp with mitotracker expressed as Mander's coefficient. **C–C.1** Immunofluorescence image showing the colocalization of Drp with mitochondria under 40×magnification. Right panel (Drp), Middle panel (Mitotracker), Left panel(merge image). Scatter plot with bar graph showing the relative overlap of Drp with mitotracker expressed as Mander's coefficient. Right panel (Drp), Middle panel (Mitotracker), Left panel (merge image). Scatter plot with bar graph showing the relative overlap of Drp with mitotracker expressed as Mander's coefficient. *Comparisons between groups were done by using one-way ANOVA followed by "Bonferroni's multiple comparison post-hoc test". p-value on figure indicates significance # $p<0.05$, ### $p<0.01$,### $p<0.001$ vs.T2DM. p-value on figure indicates significance *$p<0.05$, **$p<0.01$,***$p<0.001$ vs. BSA and NC and # $p<0.05$, ##$p<0.01$, ### $p<0.001$ vs. P-200 and T2DM*

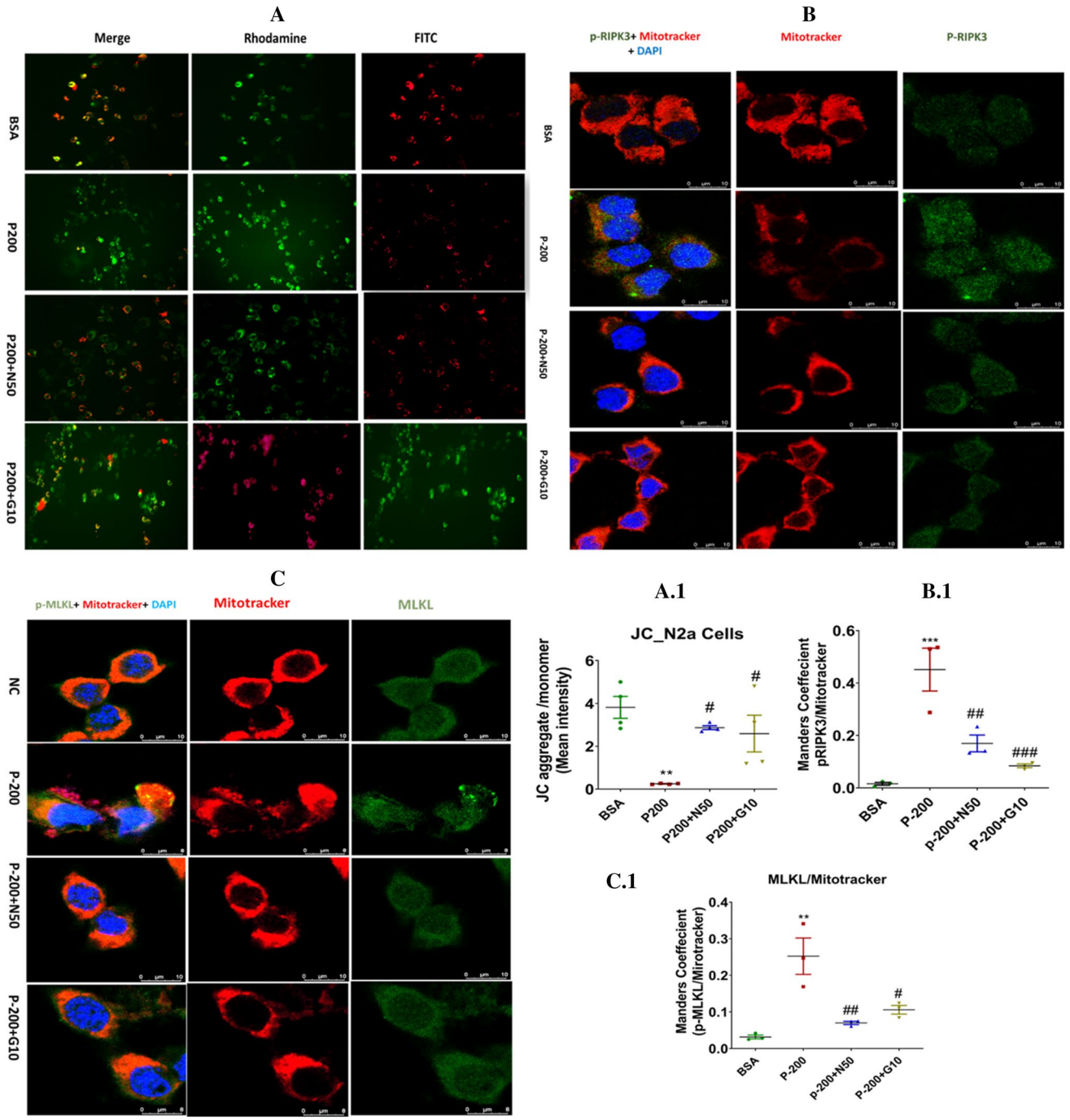

Fig. 9 Effect of Nec-1S and GSK-872 on mitochondrial membrane potential and p-RIPK3 and p-MLKL colocalization to mitochondria. **A-A.1** Fluorescent image showing JC1 stain of N2A Cell, right panel (JC 1 aggregate, red color), middle panel (JC monomer, green color), left panel (merge image), Scatter plot shows the relative ratio of JC aggregate to JC monomer between BSA, P200, P200 + N50, P200 + G10. **B-B.1** Immunofluorescence image showing the colocalization of p-RIPK3 with mitochondria under 40 × magnification. Right panel (p-RIPK3), Middle panel (Mitotracker), Left panel(merge image). Scatter plot with bar graph showing the relative overlap of p-RIPK3 with mitotracker expressed as the Mander's coefficient. **C–C.1** Immunofluorescence image showing the colocalization of p-MLKL with mitochondria under 40 × magnification. Right panel (p-MLKL), Middle panel (Mitotracker), Left panel(merge image). Scatter plot with bar graph showing the relative overlap of p-MLKL with mitotracker expressed as the Mander's coefficient. *Comparisons between groups were done by using the one-way ANOVA followed by "Bonferroni's multiple comparison post-hoc test". p-value on figure indicates significance *p < 0.05, **p < 0.01,***p < 0.001 vs. BSA and, # p < 0.05, ##p < 0.01, ## p < 0.001vs. P-200*

We also evaluated the Nec-1S and GSK-872 effect on mitochondrial enrichens with RIPK3 and later Drp aggregating with mitochondria under lipotoxic stress in cells and the tissue as well. To evaluate the mitochondrial enrichens with RIPK3, we performed a p-RIPK3 colocalization study with a mitotracker.P-200 has significantly increased ($p = 0.0007$) the p-RIPK3 mean intensity. Both have decreased the percentage overlap with mitotracker N50 ($p = 0.0118$), and G10($p = 0.0022$) (Fig. 9 B-B.1). The diabetic brain has shown an increase in the total Drp expression in the hippocampus ($p = 0.0021$) compared to normal. Nec-1S treatment has decreased the DRP expression but the decrease was not significant ($p = 0.4032$) compared to the diabetic brain (Fig. 8 A, A.1). The Drp expression at the mRNA level was also found to be increased ($p = 0.0012$) in the diabetic brain compared to normal. However, Nec-1S treatment did not show a significant change (Fig. 8 A2). The colocalization study between mitotracker dye and Drp in the tissue section has shown increased yellow puncta formation or Drp-positive mitochondria in the diseased brain ($p = 0.0064$) compared to normal whereas the Nec-1S treatment has significantly decreased the DRP-positive mitotracker(Fig. 8 B-B.1). The P-200 has also significantly increased the Pearson coefficient for Drp-mitotracker colocalization ($p < 0.0001$) whereas both N-50 and G-10 have diminished the Drp concentrates in mitochondria ($p < 0.0001$) (Fig. 8 C-C1). The present section tries to correlate mitochondrial interrelation to necroptosis. We have managed to show that p-MLKL does interact with mitochondria which might lead to the leakage of mitochondrial contents into the cytoplasm and jetting off various other signaling mechanisms. Further investigation is needed to fully decipher the mitochondrial interrelationship to necroptosis.

Based on the recent report loss of autophagy and lysosomal clearance mechanism is related to necroptosis. The loss of autophagy was reported to be involved in the RIPK-mediated transition from apoptosis to necroptosis (Goodall et al. 2016). An increase in the p62 level and the conversion of LC3B-I to II conveys ongoing autophagy. However, their clearance depends on lysosome function, and hence the defective clearance is also a pathological marker per se. There are previous reports supporting the defective clearance of diabetic brain and later has been associated with imbalanced DRP-mediated mitochondrial fission (Park et al. 2021). To explore this, we have evaluated the p62 level, which was found to be increased in the disease hippocampus tissue($p = 0.0030$) The Nec-1S treatment significantly decreased the p62 level in the hippo ($p = 0.0043$) (Fig. 10 A-A1). Although we could not analyze the RIPK to p62 interaction and vice-versa, however, the p-RIPK to LAMP-1 colocalization study revealed the inverse relationship. The diseased brain has shown a decrease in the LAMP-1 positive neuron compared to the normal control($p = 0.0006$). Firstly Nec-1S treatment significantly increases the LAMP-1 ($p = 0.0080$) positive neuron compared to diabetic brain. Further, the percentage overlap of LAMP-1 to p-RIPK was elevated and Nec-1S treatment significantly decreased ($p = 0.0021$) the same (Fig. 10C, C1-2). However, the LAMP-1 level at the mRNA level was found to be elevated in the diseased brain($p = 0.0008$) whereas there was no significant change was observed in the Nec-1S treated brain($p = 5417$)(Fig. 10 B). Meanwhile, Whether the p-RIPK/LAMP-1 scenario is one of the initial events, or it's the aftereffect of p-MLKL-mediated lysosomal damage still needs to be explored further. To evaluate p-MLKL association with the lysosome, we performed a colocalization study of p-MLKL with LAMP-1 A significant increase in p-MLKL-LAMP-1 puncta formation was observed in the diseased brain($p < 0.001$ whereas Nec-1S treatment decreased the puncta formation ($p = 0.0004$) and increased the cyton-specific LAMP-1 expression (Fig. 11 A-A. 1). The LAMP-1/LC3 colocalization study has shown that Nec-1S treatment significantly increases the colocalization of LAMP-1/LC3 ($p = 0.0007$) measured as Pearson coefficient, which was diminished in the diseased brain (Fig. 11 B -B.1). The p62 mean intensity was also found to be more with a concomitant decrease in LAMP-2 in the diabetic brain, showing impaired lysosomal clearance. which was significantly restored in the Nec1S-treated brain ($p = 0.0053$). moreover, p62 relative overlap with LAMP-2 was also elevated in Nec-1S treated brain ($p = 0.0050$)(Fig. 12 A, A1-2). Later was also evaluated in N2A cells under P-200 significantly increasing the p62 expression ($p = 0.0010$) with diminished LAMP-2 mediated clearance. Later we also observed that Nec-1S at the dose of N50 decreases the p62 mean intensity ($p = 0.0053$)and improved the lysosomal clearance as evidenced by Mander's coefficient depicting the relative overlap of p62 with LAMP2. ($p < 0.0001$) (Fig. 15B, B1-2).

Nec-1S alleviated the disease-associated microglial-like changes and their neuroinflammatory response in tissue and BV2 cells

Earlier we have shown p-MLKL, and p-RIPK3 colocalizing with IBA as well. Moreover, elevated mean intensity of IBA was also observed in the diabetic brain. The canonical pathway of necroptosis is TNFR-mediated RIPK1 activation. The present study immunoreactivity study has shown an increase in the TNFR reactivity in the brain compared to normal control ($p = 0.0027$) and the Nec-1S has significantly decreased the same($p = 0.0050$). Moreover, the colocalization study of IBA with TNFR has also shown an increase in the mender's coefficient in the diabetic brain ($p = 0.0032$), and the same was significantly decreased in the treated brain($p = 0.0028$) (Fig. 12 A, A1-2). Meanwhile, TNFR was also observed

other than IBA positive region which possibly tells that the latter is also very much present on the neuron and astrocyte.

To further decipher the changes in DAM, we carried out a western blot analysis of some markers associated with the pro and inflammatory nature of microglia. The major contributing factor to neuroinflammation, an elevated level of p-NF-Kβ ($p = 0.0005$) was observed whereas treatment has significantly decreased the level($p = 0.0064$). As per the previously published data, suppression of the p-NF-κβ signaling pathway by antioxidant have alleviated the diabetes-associated cognitive deficit (Kuhad et al. 2009). Based on the previous study, cytokines such as TNF-α, IL-6, and IL-1β along with NOS-II expression are associated with inflammation, whereas IL-4 and arginine are often linked with the antiinflammatory nature of microglia (Chang et al. 2018). The diabetic brain is also associated with neuroinflammation with elevated proinflammatory cytokines such as TNF-α, interleukins IL-6, and a decrease in the IL-4 (Table 2). Here we have found that Nec-1S treatment has significantly diminished the NOS-II expression in the hippocampus ($p = 0.0372$) compared to the diabetic brain which has significantly increased levels of the same ($p = 0.0086$) compared to the normal control brain. The NOS-II mRNA level was also found to be elevated in the diseased brain ($p = 0.0015$) whereas the Nec-1S treated has shown significantly diminished the same ($p = 0.0110$). The diabetic brain has shown a significant decrease in the arginase-expressing microglia in the (hippocampus ($p = 0.0053$), The level of which was not changed in the treatment as well. (Fig. 13B-B1). The RT-PCR study revealed an increase in the mRNA fold change of TNF-α($p = 0.0007$), IL-6($p = 0.0007$), and IL-1β ($p = 0.0076$) in the diabetic brain, which was significantly lowered in the treated brain, TNF ($p = 0.0067$), IL-6 ($p = 0.0036$), IL-1β ($P = 0.0300$) (Fig. 13 C).

Further, we used CD16/32, and CD206, the 2 surface markers to illustrate their expression pattern by using a double immunofluorescence labeling study in the diseased and treated brain section. An increase in CD16 and a decrease in CD206 are associated with the inflammatory state of DAM and vice versa (Sen et al. 2020). We have found an increase in CD16/IBA overlap coefficient in the hippocampus compared to normal control ($p < 0.001$) whereas the Nec-1S treatment has decreased the CD16 positive cell ($p = 0.0033$) compared to the treated group. Whereas the latter has shown a significant increase in CD206/IBA overlap coefficient in the hippocampus as well ($p = 0.0012$). Moreover, the treated group has also shown a decrease in the C16 positive to CD206 microglia ratio ($p < 0.01$) (Fig. 14 A, A1-3). DAM characteristics are also based on the cytokine in their milieu, IL-6 led to the inflammatory nature of microglia whereas IL-4 promotes the anti-inflammatory or protective microglia. However, the above correlation is not direct per se and various other factors and most importantly duration of any stress might affect the cytokine profile and microglial change (Zhao et al. 2015). Referring to the result in (Fig. 3E-G) 24-h treatment of PA-BSA conjugate to N2A cell increases the IL-6 level which is consistent with belief that IL-6 increases under T2DM or lipotoxicity to say. Whereas the IL-4 level did not show a decrease under 24 h., rather P-300 exposure has slightly increased the level of the same.

To elaborate on the lipotoxicity effect at the cellular level we used BV2 cells. PA-BSA working dose and Nec-1S dose were decided on the cell viability based -on the MTT test (S-3,a-d) and western blot analysis. The 24 h. exposure of PA-BSA conjugate has also increased the p-RIPK1,p-MLKL, p-NFKB, and MHC-II expression, whereas decreased ARG expression (Fig. 15B-1). For further experiments, N-50 and N-25 were considered. JC-1 staining assay was performed to evaluate the Change in MMP(Ψm). The P-200 has significantly decreased the JC aggregate/monomer ratio ($p = 0.0005$) compared to the vehicle-treated group. Both the dose of N-50($p = 0.0095$) and N-25($p = 0.0246$) have managed to maintain the MMP (Fig. 15 A-A1). Next, we carried out the western blot analysis for p-RIPK, p-RIPK3, p-MLKL, NOS-II, P-NFKβ, and NOS-II. P-200 significantly increase the p-RIPK($p = 0.0025$), p-RIPK3($p = 0.0004$), p-MLKL ($p < 0.0001$), NOS-II ($p < 0.0001$), P-NFKβ ($p < 0.0001$), MHC-II($p < 0.0001$) expression. Both the dose of N-50 and N-25 have been able to prevent necroptosis execution. However, the N-25 dose did not bring any change in NOS-II ($p = 0.9999$) expression and has brought little change in MHC-II expression ($p = 0.0317$) as well (Fig. 16 A-B).

Discussion

Patients with obesity and T2DM show central nervous system (CNS) changes with reduced cerebral volume, and atrophy of mostly cortex and hippocampus.T2DM model based on HFD intake induces cognitive changes and further accelerates AD pathology(Takeda et al. 2010; Jeon et al. 2012). In earlier studies, increased PA levels in the brain have been observed in mice fed on HFD, and later linked with BBB damage (Takechi et al. 2017; Spinelli et al. 2017). In recent studies increased PA levels were linked to central inflammation and impaired insulin signaling in overweight humans with diabetes, and dyslipidemia, contributing to decreased cognitive performance, and increased incidence of glia activation (Melo et al. 2020). Cognitive decline can be linked with synaptic infidelity and neuroinflammation. The synaptic weakening can be linked to glia-mediated damage and excitatory/ inhibitory neurotransmitter imbalance at the hippocampus where the information inputs occur from the cortical region. As uptake of FFA increase was observed in the hippocampus of the obesity-based

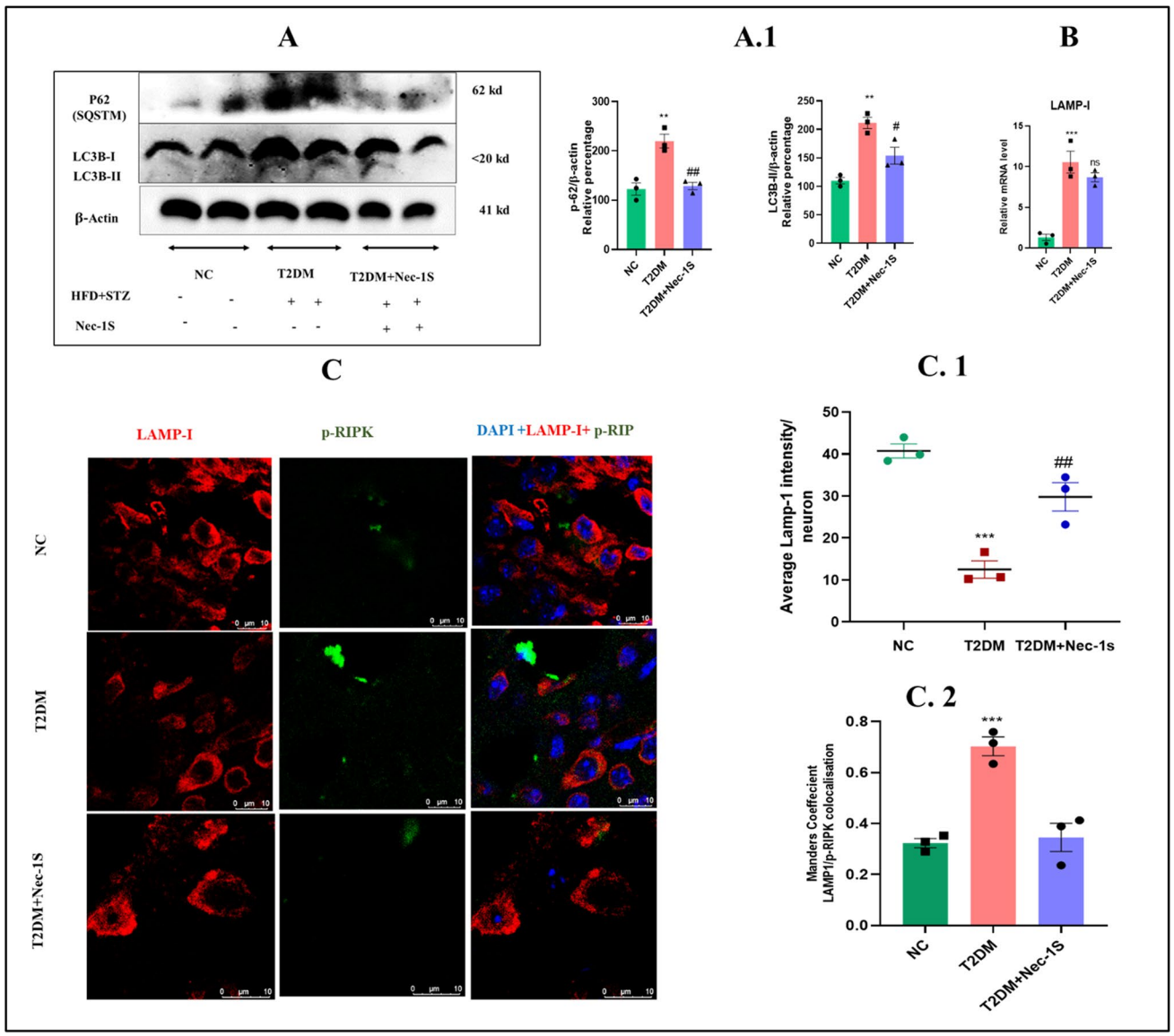

Fig. 10 Necroptosis interrelation to autophago-lysosomal mediated clearance. Effect of Nec-1S on autophagic clearance p-RIPK1/LAMP-1 colocalization. **A-A1** Western blot image of p62 and LC3B in the hippocampus tissue and scatter plot with bar graph representing the relative percentage of blot density between groups ($n=3$). **B.** Relative mRNA level of LAMP-1. **C, C1-C2** Immunofluorescence image showing colocalization of p-RIPK to LAMP-1 in the brain of NC, T2DM, and T2DM + Nec-1S under 63 × magnification, left panel (LAMP-1), Middle (p-RIPK), Right Panel(Merge). Scatter plot with bar graph showing the mean intensity of LAMP-1 and scatter plot showing the relative overlap of LAMP-1 to p-RIPK represented in the form of Mander's coefficient ($n=3$). *Comparisons between groups were done by using the one-way ANOVA followed by "Bonferroni's multiple comparison post-hoc test". p-value on figure indicates significance of* $*p<0.05$, $**p<0.01$, $***p<0.001$ *vs. NC.* $\#p<0.05$, $\#\#p<0.01$, $\#\#\#p<0.001$ *vs. T2DM*

experimental model, PA-BSA conjugate is used for mechanistic study at the cellular level. Consistent with the report, the present study reports that (i) T2DM-associated metabolic syndrome affects CNS leading to cognitive decrement involving neurodegenerative changes, and DAM-like morphological characteristics in the hippocampus whereas PA-BSA conjugate induces the same pathological hallmark in N2A and BV2 cells at the cellular level (ii)The ongoing necroptosis is the main culprit behind the CNS changes as increased protein and mRNA level of p-RIPK, p-RIPK3, p-MLKL, were observed, (iii) Nec-1S, a small molecule alleviated the cognitive decrement and decreases the incidence of neurodegenerative neuron, phosphorylated-tau, amyloid oligomer deposit and DAM like changes (iv) executioner of necroptosis also brings out the perturbation in mitochondria and autophagy process at the subcellular level leading to increased mitochondrial fission, oxidative

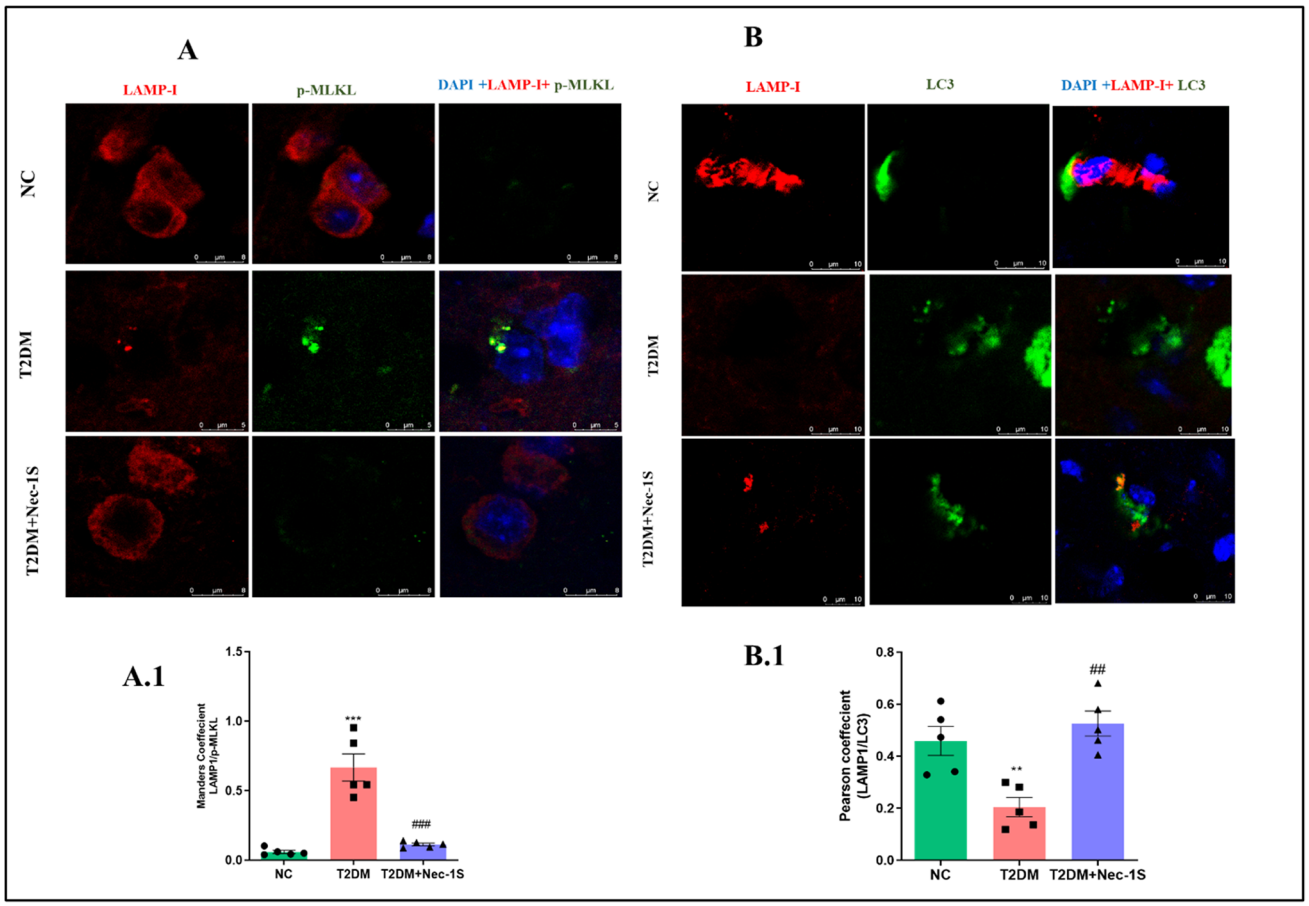

Fig. 11 Necroptosis interrelation to autophago-lysosomal mediated clearance. Effect of Nec-1S on autophagy in tissue, p-MLKL/LAMP-1 & LC3B/LAMP-1 colocalisation. **A-A1,** Immunofluorescence image showing colocalization of p-MLKL to LAMP-1 in the brain of NC, T2DM, and T2DM + Nec-1S under 63 × magnification, left panel (LAMP-1), Middle (p-MLKL), Right Panel(Merge).Bar graph showing the relative overlap of the p-MLKL to LAMP-1 represented in the form of Mander's coefficient ($n = 3$). **B1-2** Immunofluorescence image showing colocalization of LC3B to LAMP-1 in the brain of NC, T2DM, and T2DM + Nec-1S under 63 × magnification, left panel(LAMP-1), Middle (LC3B), Right Panel(Merge). Bar graph showing the relative overlap of the p-MLKL to LAMP-1 represented in the form of Mander's coefficient ($n = 3$). *Comparisons between groups were done by using the one-way ANOVA followed by "Bonferroni's multiple comparison post-hoc test". p-value on figure indicates significance of* $^{*}p < 0.05$, $^{**}p < 0.01$, $^{***}p < 0.001$ *vs. NC. p-value on figure indicates significance* $\#p < 0.05$, $\#\#p < 0.01$, $\#\#\#p < 0.001$ *vs. T2DM*

stress and failure of autophagolysosomal fusion and toxic clearance.

The present study does not cater to the aspect of how RIPK-mediated necroptosis starts. However, various theories have been postulated, such as TNF-mediated via interaction with TNFR-led to RIPK and its downstream execution of necroptosis. One of them is lysosomal damage could lead to RIPK, RIPK3 accumulation(Liu et al. 2018), ubiquitination of RIPK(Roberts et al. 2022), decrease in Tank Binding Protein (TBK) activity (Xu et al. 2018), or autophagic failure leading to p62 recruitment of RIPK1(Goodall et al. 2016). However, we found a negative correlation between LAMP-1 and p-RIPK expression patterns in the diseased brain implying that RIPK1-positive neuron has specifically decreased expression. On investigating the probability for TNF-mediated necroptosis, the TNFR expression was accentuated on the microglia of the diseased brain as evidenced by the colocalization study between IBA and TNFR. Moreover, the TNFR expression can be observed other than IBA implying, the involvement of other TNFR- mediated signaling in neighbor cells as well. In the present study, the necroptosis mechanism is evident majorly in neurons and microglia. Previously HFD fed mice have shown an increase in amyloid plaque and phosphorylated-Tau deposit due to PA-BSA conjugate mediated increase in (Amyloid converting enzyme) BACE and (amyloid precursor proteins) APP expression(Kim et al. 2017). Necrosome is also an amyloid-like structure and Nec-1S targets necrosome assembly, Aβ plaque formation, and Phosphorylated Tau deposit further alleviating cognitive impairment (Yang et al. 2017). Nec-1S preserved the patency of cerebral endothelium, BBB integrity, and cognitive ability and decreased the Aβ deposit in

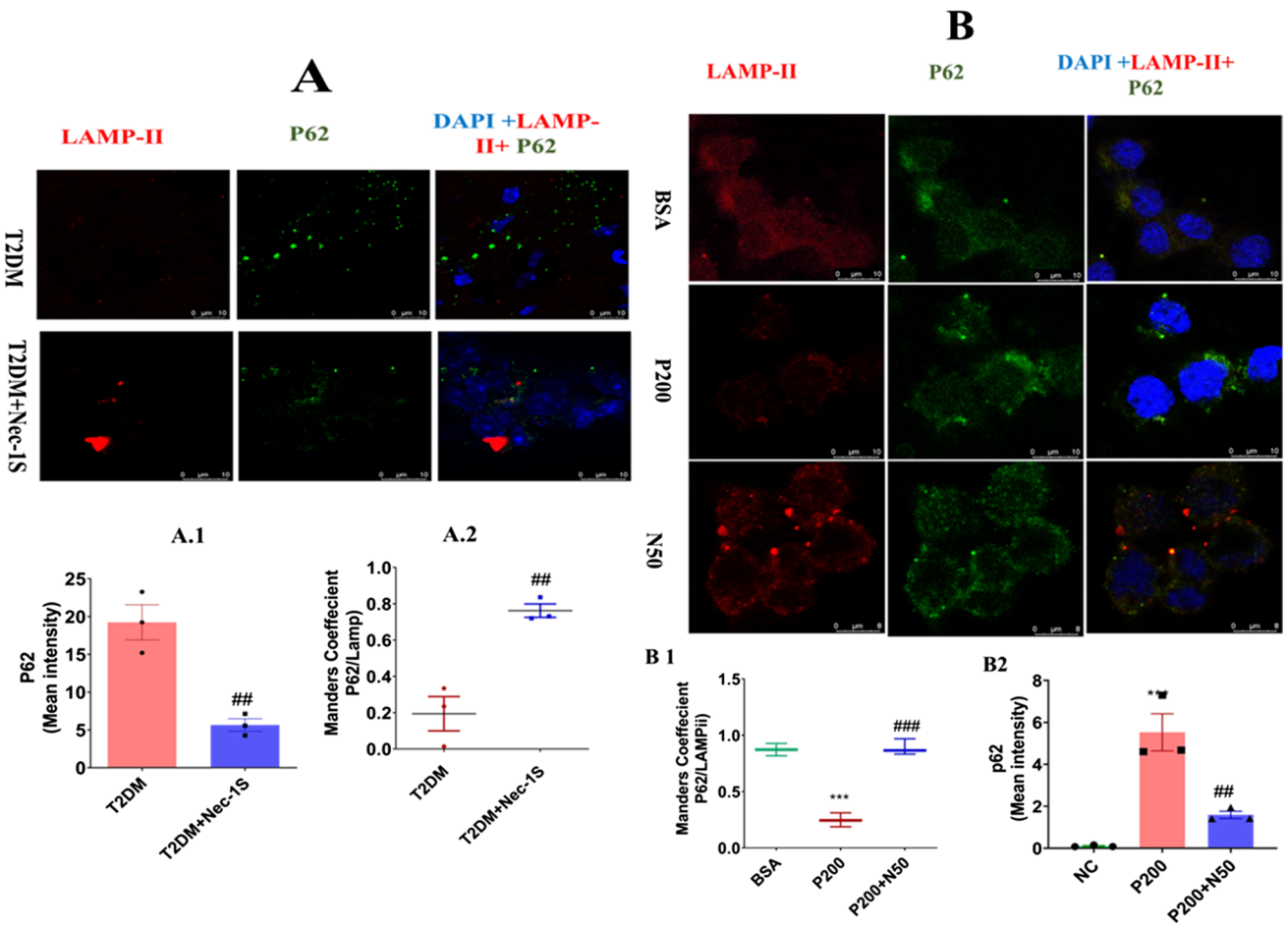

Fig. 12 Necroptosis interrelation to autophago-lysosomal mediated clearance. Effect of Nec-1S on autophagy in tissue and N2A cells p62/LAMP-2 colocalization. **A-A1-2** Immunofluorescence image showing colocalization of p62 to LAMP-2 in the brain of T2DM and T2DM + Nec-1S under 63 × magnification, Right panel (p62), Middle(LAMP-1), Left Panel(Merge). Bar graph showing the relative overlap of the p62 to LAMP-2 represented in the form of Mander's coefficient ($n = 3$). **6.3 B, B1-2** Immunofluorescence image showing colocalization of p62 to LAMP-2 in N2A cell under 40 × magnification, Right panel(p62), Middle(LAMP-2), Left Panel(Merge). Scatter plot with bar graph showing the relative overlap of the p62 to LAMP-2 represented in the form of Mander's coefficient. ($n = 3$). *Comparisons between groups were done by using the two-tailed unpaired t-test. p-value on figure indicates significance #p < 0.05, ##p < 0.01,###p < 0.01 vs. T2DM. Comparisons between groups were done by using the one-way ANOVA followed by "Bonferroni's multiple comparison post-hoc test". p-value on figure indicates significance *p < 0.05, **p < 0.001,***p < 0.001 vs. BSA and, # P < 0.05, ##P < 0.01, ### p < 0.001 vs. P200*

an experimental model of the aluminum-induced mouse model AD, and T2DM-associated insulin resistance (Zou et al. 2020). In the present study also, Nec-1S shows neuroprotection, evidenced by decreased amyloid oligomer, and phosphorylated Tau deposit. Besides the expression of synaptic marker protein, synaptophysin expression was also improved in the Nec-1S-treated brain. The Nec-1S effect on apoptosis is explained differently by investigators. One such study supports the antiapoptotic effect of Nec-1S by showing increased expression of the anti-apoptotic protein Bcl-2, decreased expression of pro-apoptotic protein Bax, including cytochrome-c, and cleaved caspase-3 in cells and tissues as well in response to Aβ-induced toxicity(Yang et al. 2017). In contrast, Nec-1S did not affect apoptosis in cells exposed to TNF and IMQ-induced psoriasiform dermatitis(Duan et al. 2020). We also report here the antiapoptotic effect of Nec-1S, which could be due to its antioxidant property.

In many cases, necroptosis was interlinked with mitochondrial dysfunction. The MLKL probably after translocating to mitochondria, further impairs the oxidant/antioxidant balance and progresses the cellular damage(Chen et al. 2014; Ding et al. 2019; Li et al. 2021). However, this could be perceived as the primary event as T2DM-associated biochemical perturbation itself disturbs the oxidant/antioxidant balance. There is another theory that explains damaged mitochondria also initiate necroptosis via DAMPs. Mitochondrial dysfunction has been closely associated with AD (Preeti et al. 2021), PD, Spinal cord injury(Jiao et al.

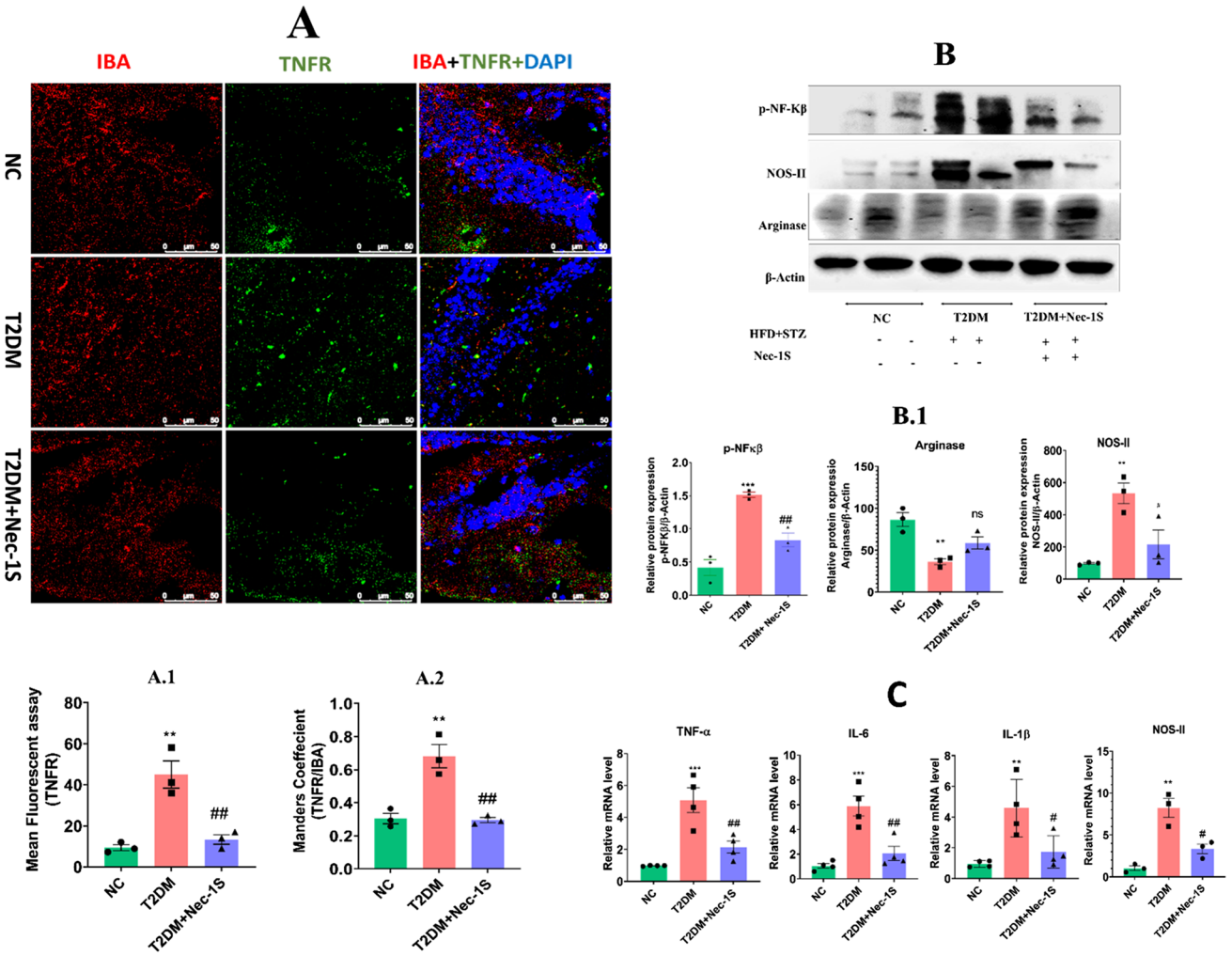

Fig. 13 Nec-1S effect on protein expression of disease-associated microglia in the hippocampus. **A**-Immunofluorescence image showing the colocalization between IBA and TNFR**.** Left panel (microglia labeled with IBA), Middle panel (TNFR) Right panel (Merge image) of the hippocampus of NC, T2DM, and T2DM + Nec-1S group. A1-2 Mean fluorescence intensity of TNFR and scatter plot with Bar graph showing the relative overlap of the TNFR to IBA represented in the form of Mander's coefficient ($n = 3$). **B-B1** Western blot image of p-NF-Kβ, NOS-II, and Arginase-I in the hippocampus tissue. Scatter plot with bar graph representing the relative percentage of blot density between NC, T2DM, and T2DM + Nec-1S.($n = 3$). **C.** Relative mRNA fold change in TNF-α, IL-6, IL-1β, and NOS-II between groups. *Comparisons between groups were done by using one-way ANOVA followed by "Bonferroni's multiple comparison post-hoc test". p-value on the figure indicates significance, *#p < 0.05, **p < 0.01, ***p < 0.001 vs. NC. #p < 0.05, ##p < 0.01, ###p < 0.001 vs. T2DM*

2020), TBI, and ischemic reperfusion injury (Zhou et al. n.d.). Bax and Bcl-2 are regarded as possible indicators of mitochondrial dysfunction whereas TFAM is an indicator of mitochondrial-dependent transcriptional efficiency that contributes to the cellular response under stress and is related to neurodegenerative disorder (NDDs) (D'Orsi et al. 2017; Li et al. 2017; Roberts et al. 2022). Earlier antioxidants did not reverse the lipotoxicity-induced mitochondrial dysfunction, mtDNA leakage, and cell death (Patková et al. 2014). However, we have shown here both Nec-1S, and GSK-872 prevent the p-MLKL translocation to mitochondria and MMPs alteration in cells under lipotoxic stress. The RIPK3- is also responsible for Drp phosphorylation via activating the PGAM5. Drp contributes to mitochondrial fragmentation, ultimately disturbing their homeostasis. RIPK3 inhibition has alleviated the necroptosis-mediated energy disruption in acute microvascular ischemia–reperfusion injury (Zhou et al. n.d.).The present did not present the data on p-DRP. Nonetheless, here Nec-1S and GSK872 both alleviated the RIPK3 translocation and later Drp concentrating in mitochondria under lipotoxic stress. The Drp colocalization with mitochondria was also observed in the hippocampal region of the diabetic brain. Moreover, the Drp expression was also elevated at the mRNA level. Hence inhibiting necroptosis

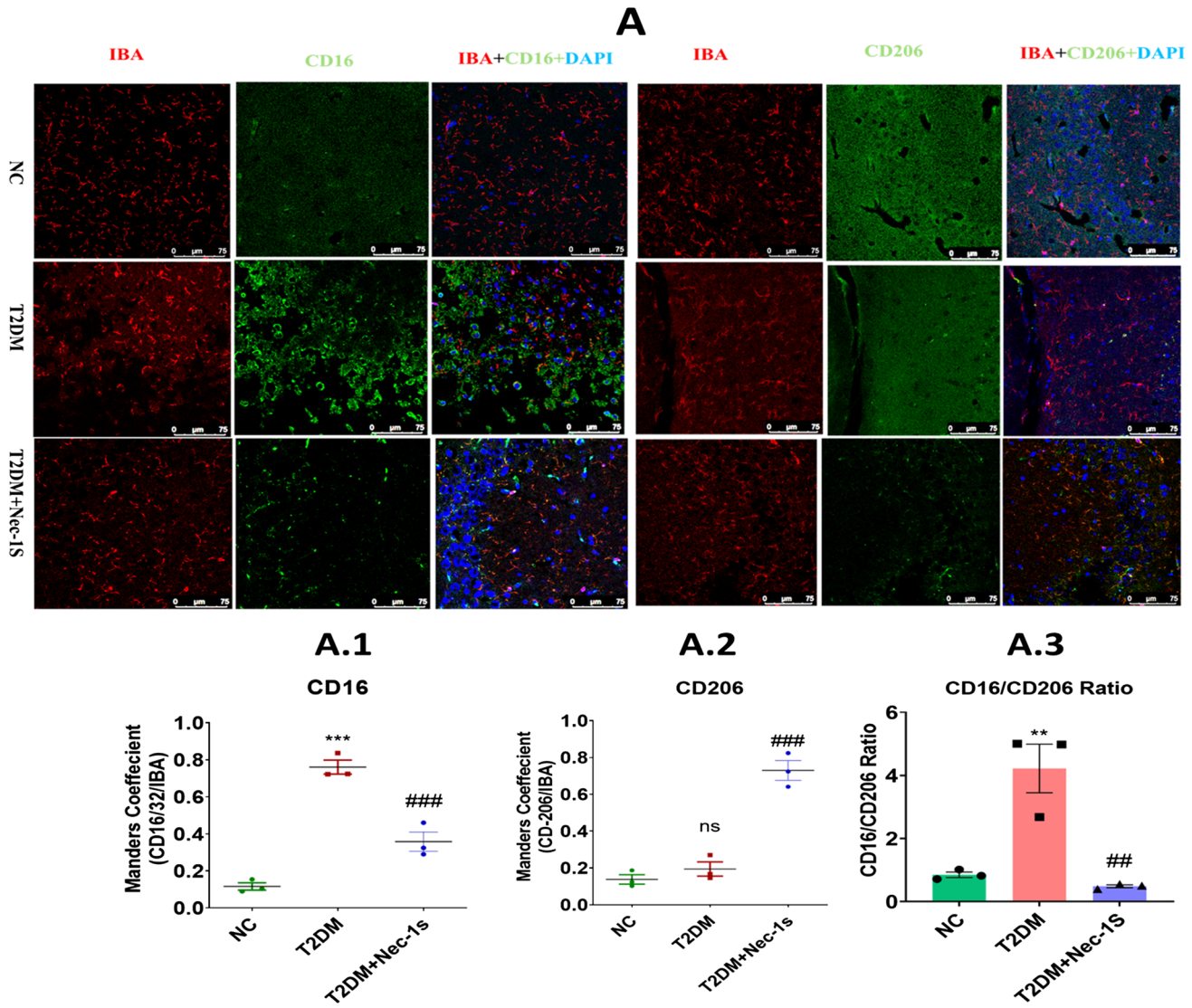

Fig. 14 Nec-1 s effect on the microglia-specific CD marker in the tissue. **6.2A, A1-2** Immunofluorescence image showing colocalization of CD16 and CD206 to IBA in the hippocampus of NC, T2DM, and T2DM + Nec-1S under 40 × magnification, and the Scatter plot with bar graph showing the relative overlap of the CD16 and CD206 to IBA represented in the form of Mander's coefficient. ($n = 3$). **A. 3** Scatter plot with bar graph showing the ratio of relative overlap of the CD16 and CD206 to IBA. *Comparisons between groups were done by using the one-way ANOVA test. p-value on the figure indicates significance #p < 0.05, ##p < 0.01,###p < 0.001 vs. T2DM. p-value on figure indicates significance *p < 0.05, **p < 0.01,***p < 0.001 vs. BSA and, # p < 0.05, ##P < 0.01, ### p < 0.001 vs. P-200*

has potentially blocked further cellular damage by maintaining mitochondrial integrity. The above finding explains necroptosis after-effect on mitochondria. Meanwhile, later needs elaborate studies for further clarification.

Metabolic stress and other aging-related CNS disorders are associated with protein inclusion formation. The aberrant protein inclusion deposit along with constitutive autophagic machinery loss, considered responsible for the removal of aberrant protein is long been considered the underline mechanism behind impaired brain functioning. Autophagy is a complex process, its execution is still debatable regarding how exactly it functions, and whether alleviating or potentiating autophagy would be beneficial as therapy. Moreover, lysosomal clearance is an important aspect of autophagic clearance. The increasing evidence has always supported the idea of promoting autophagy, especially in immune-metabolic disorders, neurodegenerative diseases, and cancer. There are various regulators, and proteins involved in autophagy such as p62, LC3B and further LAMP 1/2 assisted autophago-lysosome formation. Autophagic loss is characterized by increased accumulation of p62, lipidated LC3B, and failure of autophagosome formation. Here we have also shown the increase in p62 level in the hippocampus, and

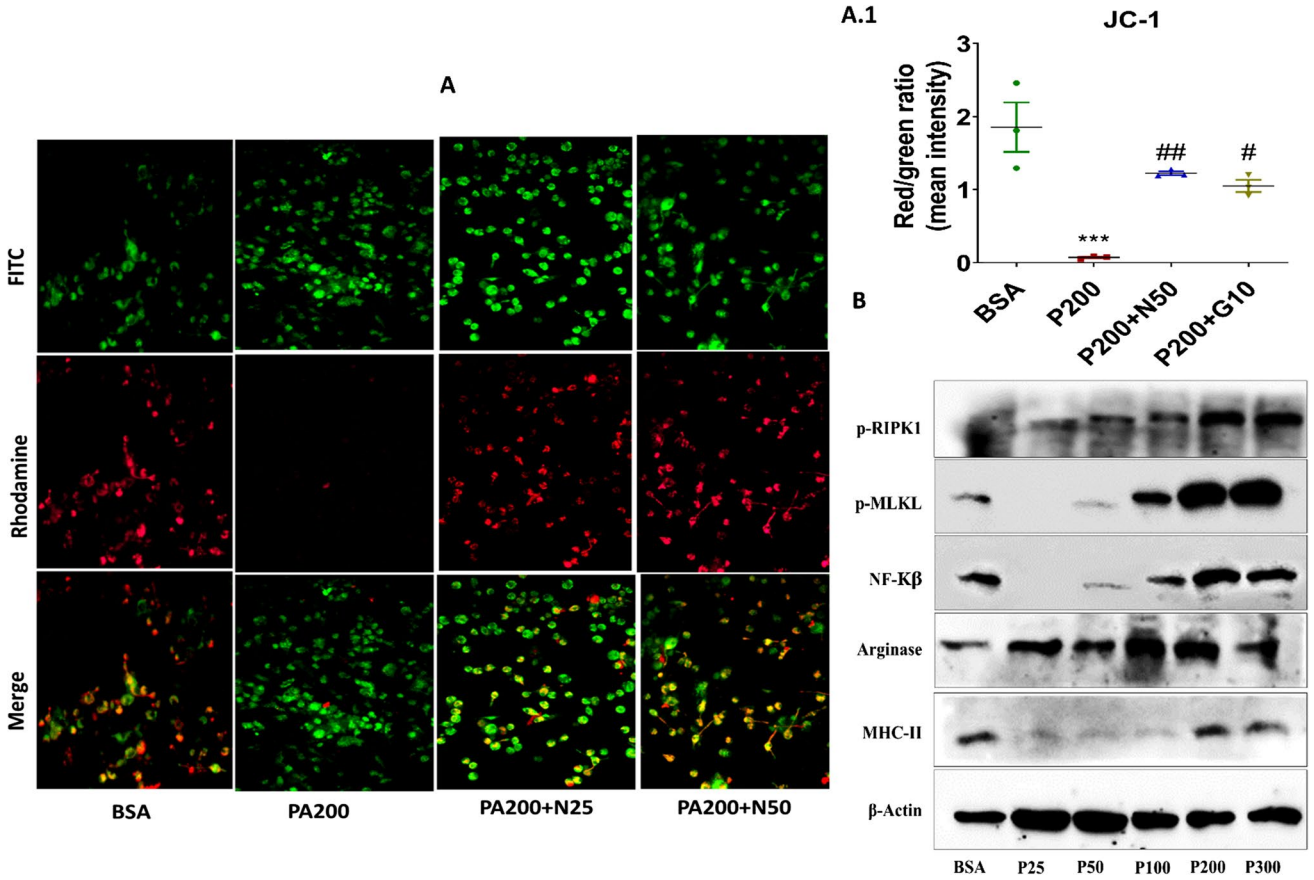

Fig. 15 Effect of lipotoxicity on and Nec-1S on microglial-specific necroptosis and mitochondrial membrane potential. **A-A1** Fluorescent image showing JC1 stain of Cell, upper panel (JC 1 monomer, green color), middle panel (JC aggregate, red color), lower panel (merge image), Scatter plot shows the relative ratio of JC aggregate to JC monomer between BSA, P200, P200 + N50, P200 + N25. **B** Western blot image of p-RIPK, p-MLKL, p- MHC-II, Arginase, p-NF-Kβ in BV2 cell. P-25, P-50, P-100, P-200,P-300 vs. BSA group (vehicle)

PA-BSA conjugate exposed cells. Lysosomes are the ultimate destination for autophagic cargo degradation and hence lysosomal dysfunction led to inefficient autophagic cargo degradation. A decrease in LAMP 1/2 and LC3-LAMP-1 puncta formation is closely associated with AD-like neurite plaque formation and decreased hippocampal functioning (Rothaug et al. 2015; Yao et al. 2018). In contrast, axonal deposition of luminal protease deficient LAMP-1 in response to Aβ deposit was also reported in AD (Gowrishankar et al. 2015; Sharoar et al. 2021). HFD ingestion and PA exposure have inhibited the autophagic flux process in totality and impaired autophagosome-lysosome fusion and end lysosomal dynamics in the hypothalamus and hypothalamic neuron. p-MLKL upon activation also compromises the autophagy process(Frank et al. 2019), meanwhile, RIPK1 also can have a direct effect on autophagy. In the present study, p-MLKL-LAMP-1 puncta were visible with a concomitant decrease in LAMP-1 intensity.Nec-1S treated brain has shown improved LAMP-1 expression, especially in the neuronal cyton and not in the axon, probably due to decreased p-MLKL translocation to the lysosome. Further LC3B/LAMP-1 puncta were also affected in the diabetic brain which depicts the failure of autophagolysosomal formation. We have also observed a decrease in LAMP-2 expression in hippocampal, cortical tissue, and neuronal cells. Nec-1S not only decreases the p62 level but, also increases the p62-positive LAMP-1 expression along with the lipidated LC3B in hippocampus tissue. Although the present work does not explore the detailed mechanism and relative role of p-RIPK, p-RIPK3, and p-MLKL in the context of autophagolysosomal mediated clearance mechanism, it certainly opens the idea for exploration under T2DM or lipotoxicity stress. The DAM is being used in the context of changes in microglial characteristics associated with disease states. Many investigators have used the M1/M2 paradigm while discussing the microglia, but the dichotomy around the terminology is persisted and now new roadmaps are being advised to nominate the microglia (Paolicelli et al. 2022). T2DM is a chronic metabolic disease that led to neuroinflammation due to various cytokines released by immune cells. Changes in the metabolite profile and egression of peripheral inflammatory mediators due to BBB damage also led to brain inflammation. Earlier intracerebroventricular

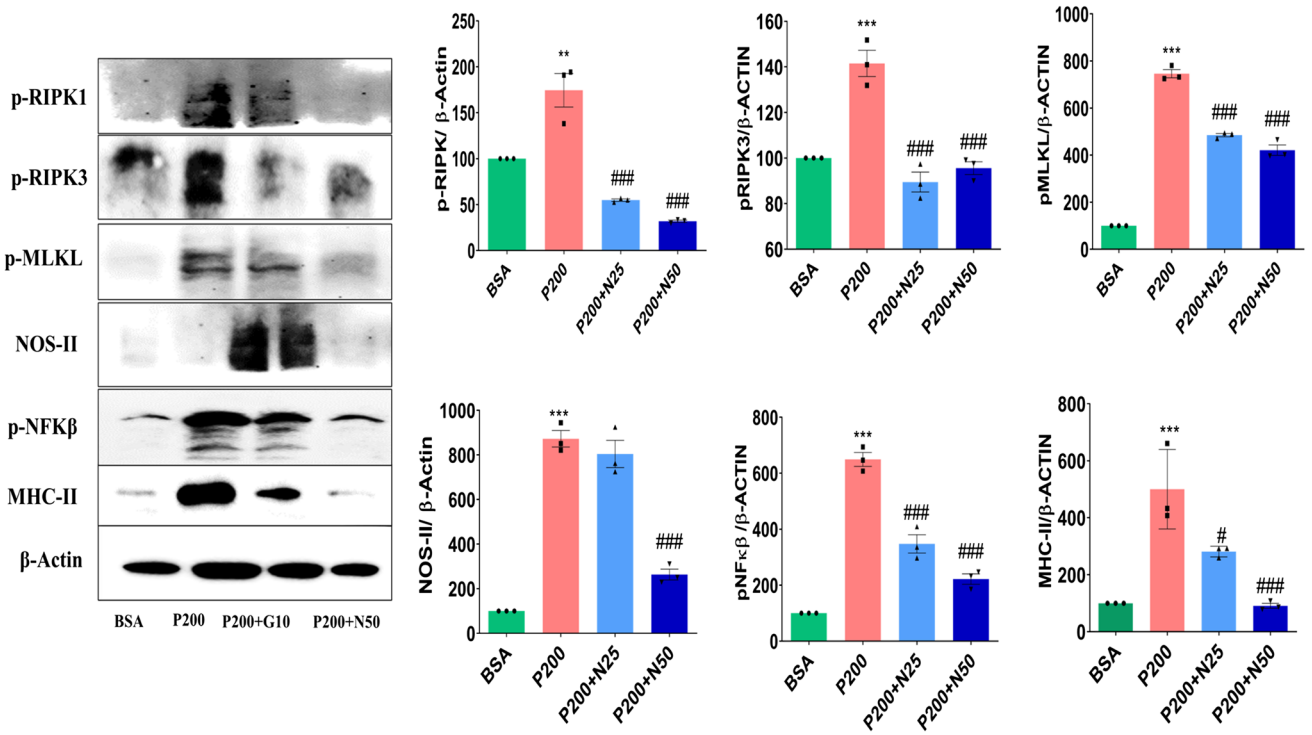

Fig. 16 Effect of Nec-1S on microglial-specific necroptosis executioners. **A-B** Western blot image of p-RIPK, p-RIPK3, p-MLKL, NOS-II, p-NFKβ, MHC-II in BV2 cell between BSA vs. P200, P200 + N25, P200 + N50. *p-value on figure indicates significance *p < 0.05,**p < 0.001,***p < 0.001 vs. BSA and, # p < 0.05, ##p < 0.01, ### p < 0.001 vs. P-200*

(ICV) administration of PA-BSA conjugate to the brain has brought the cognitive decline associated with insulin insensitivity and increased microglial and astrocytic reactivity mediated by increased TNF-α (Melo et al. 2020).As amyloid deposition progresses, as a consequence of initial events or later in response to Aβ deposit, it gets surrounded by the DAM(Preeti et al. 2021). The DAM with necroptosis also contributes to the progression of neurodegeneration (Salvadores et al. 2022). In the present study, we have shown the increased IBA reactivity associated with longer projection and swollen cyton or button-like structure in microglia in the diabetic brain. Moreover, p-MLKL and p-RIPK3 colocalize with microglia as well. Elevated cytokines such as TNF-α, IL-6, and IL-1β along with MHC-II, and NOS-II expression are associated with inflammation, whereas IL-4, arginine, and YM-1 are often linked with the antiinflammatory nature of microglia(Chang et al. 2018). Hippocampal IL4 level is positively correlated to ARG-positive microglia and BDNF-dependent neurogenesis (Melo et al. 2020). We have seen here elevated IL-6 in the supernatant of PA-BSA treated cells, hippocampal lysate. Besides the above, the expression of IL-6, TNF-α, and IL-1β at the mRNA level was also elevated. These finding further supports the ongoing neuroinflammation and neuro-glia cross-talk in accentuating the inflammatory crisis. Additionally, CD16/32, and CD206, the 2 surface markers are being attributed to different microglia/ macrophage populations (Jurga et al. 2020). An increase in CD16 and a decrease in CD 206 are associated with the inflammatory state of DAM whereas the increase in CD206 and decrease in CD16 are attributed to the protective state of DAM perse (Chang et al. 2018; (Sen et al. 2020). PA-BSA conjugate has also increased the p-RIPK1, p-MLKL, p-NFKB, NOS-II, and MHC-II expression, whereas decreased the ARG in a dose-dependent manner in BV2 cells. As discussed, earlier PA-BSA conjugate interferes with mitochondrial function and a decrease in MMP (Ψm) is related to necroptosis(Lu et al. 2019).In the present study, Nec-1S treatment has decreased the expression of NOS-II, MHC-II, and NFKβ and maintained the (Ψm). Later certainly confirms the necroptosis role in DAM. Further Nec-1S has also normalized the CD16/CD206 expression pattern towards a protective phenotype.

The present study has its share of limitations such as the underlying mechanism for necroptosis initiation, mechanistic study around amyloid and tau deposit, neuro-microglia interaction, and deciphering detailed understanding of mitochondrial and autophagy machinery. However, we have managed to profile T2DM like chronic metabolic disease-associated brain changes in the form of behavioral response, BBB changes, AD-like characteristics, necroptotic changes at the hippocampus level, as well as immune and inflammatory response. Further, we have also tried to interlink the necroptosis mechanism to the subcellular changes at the mitochondrial and autophago-lysosomal strata.

Conclusion

In summary T2DM like metabolic disease brings out changes in peripheral immune response, increases BBB permeability, cognitive decrement, central inflammatory reaction, amyloid and tau deposit, mitochondrial dysfunction, and impaired autophago-lysosomal clearance mechanism. The above changes are closely linked with necroptosis and Nec-1S has the potential to act via a multifactorial mechanism.

Supplementary Information The online version contains supplementary material available at https://doi.org/10.1007/s11011-023-01185-8.

Acknowledgements Authors would like to acknowledge the financial support provided by the Department of Pharmaceuticals, Ministry of Chemicals and Fertilizers, Government of India for carrying out the present research work.

Author contribution Ms. Kumari Preeti (Department of Pharmacology and Toxicology, NIPER-HYDERABAD, Telangana, India-500037) conceptualized and performed all the *in-vitro* and animal studies, analyzed the data, and wrote the manuscript; Ms. Valencia Fernandes and Anika Sood (Department of Pharmacology and Toxicology, NIPER-HYDERABAD, Telangana, India, 500037) have equally helped in performing experiments, analyzing, evaluating data, and reviewing the manuscript. Mr. Islauddin Khan (Department of Pharmacology and Toxicology, NIPER-HYDERABAD, Telangana, India-500037) also helped in performing animal studies and evaluating data; Dr. Dharmendra Kumar Khatri (Department of Pharmacology and Toxicology, NIPER-HYDERABAD, Telangana, India-500037), contributed to conceptualizing and designing the study, evaluating data, and reviewing the manuscript. Dr. Shashi Bala Singh (Director, Department of Pharmacology and Toxicology, NIPER-HYDERABAD, Telangana, India-500,037) contributed to project conceptualization, designing studies, evaluating data, and reviewing the manuscript.

Funding Research fellowship by National Institute of Pharmaceutical Education and Research, NIPER Hyderabad and Department of Pharmaceuticals, Ministry of Chemicals and Fertilizers, Govt. of India.

Data availability statement The data are available on request from the corresponding author upon reasonable request.

Declarations

Research involving human and animals participants All applicable international, national, and/or institutional guidelines for the care and use of animals were followed especially ARRIVE guidelines. All procedures performed in studies involving animals were by the ethical standards of the institution at which the studies were conducted (Institutional Animal Ethics Committee (IAEC)—NIPER Hyderabad, Protocol No. NIP/10/2019/PC/34.

Informed consent statement This article does not contain any studies with human participants performed by any of the authors. Not applicable.

Consent to publish Not applicable.

Conflict of interest The authors declare no conflicts of interest.

References

Amenta PS, Jallo JI, Tuma RF et al (2014) Cannabinoid receptor type-2 stimulation, blockade, and deletion alter the vascular inflammatory responses to traumatic brain injury. J Neuroinflammation 11:1–10. https://doi.org/10.1186/s12974-014-0191-6

AU J, NL S, M S, D M-R (2017) Drp1/Fis1 interaction mediates mitochondrial dysfunction, bioenergetic failure and cognitive decline in Alzheimer's disease. Oncotarget 9:6128–6143. https://doi.org/10.18632/ONCOTARGET.23640

Barrière DA, Noll C, Roussy G et al (n.d.) Combination of high-fat/high-fructose diet and low-dose streptozotocin to model long-term type-2 diabetes complications OPEN. https://doi.org/10.1038/s41598-017-18896-5

Becker JB, Prendergast BJ, Liang JW (2016) Female rats are not more variable than male rats: a meta-analysis of neuroscience studies. Biol Sex Differ 7. https://doi.org/10.1186/S13293-016-0087-5

Beery AK (n.d.) Inclusion of females does not increase variability in rodent research studies. https://doi.org/10.1016/j.cobeha.2018.06.016

Biessels GJ, Whitmer RA (2020) Cognitive dysfunction in diabetes: how to implement emerging guidelines. Diabetologia 63:3–9. https://doi.org/10.1007/S00125-019-04977-9

Bowe JE, Franklin ZJ, Hauge-Evans AC et al (2014) METABOLIC PHENOTYPING GUIDELINES: Assessing glucose homeostasis in rodent models. J Endocrinol 222:G13–G25. https://doi.org/10.1530/JOE-14-0182

Caccamo A, Branca C, Piras IS et al (2017) Necroptosis activation in Alzheimer's disease. Nat Publ Gr. https://doi.org/10.1038/nn.4608

Chakraborty A, Hegde S, Praharaj SK et al (2021) Age related prevalence of mild cognitive impairment in type 2 diabetes mellitus patients in the indian population and association of serum lipids with cognitive dysfunction. Front Endocrinol (Lausanne) 12:1739. https://doi.org/10.3389/FENDO.2021.798652/BIBTEX

Chang C, Wan J, Li Q et al (2018) HHS Public Access. 54–69. https://doi.org/10.1016/j.nbd.2017.03.016.Alternative

Chen X, Li W, Ren J et al (2014) Translocation of mixed lineage kinase domain-like protein to plasma membrane leads to necrotic cell death. Cell Res 24:105–121. https://doi.org/10.1038/CR.2013.171

D'Orsi B, Mateyka J, Prehn JHM (2017) Control of mitochondrial physiology and cell death by the Bcl-2 family proteins Bax and Bok. Neurochem Int 109:162–170

Ding Y, He C, Lu S et al (2019) MLKL contributes to shikonin-induced glioma cell necroptosis via promotion of chromatinolysis. Cancer Lett 467:58–71. https://doi.org/10.1016/J.CANLET.2019.09.007

du Sert NP, Hurst V, Ahluwalia A et al (2020) The arrive guidelines 2.0: Updated guidelines for reporting animal research. PLoS Biol 18:1–12. https://doi.org/10.1371/journal.pbio.3000410

Duan X, Liu X, Liu N et al (2020) Inhibition of keratinocyte necroptosis mediated by RIPK1/RIPK3/MLKL provides a protective effect against psoriatic inflammation. Cell Death Dis 11:1–14. https://doi.org/10.1038/s41419-020-2328-0

Frank D, Vaux DL, Murphy JM et al (2019) Activated MLKL attenuates autophagy following its translocation to intracellular membranes. J Cell Sci 132. https://doi.org/10.1242/jcs.220996

Frison E, Proust-Lima C, Mangin JF et al (2021) Diabetes mellitus and cognition. Neurology 97:e836–e848. https://doi.org/10.1212/WNL.0000000000012440

Goodall ML, Fitzwalter BE, Zahedi S et al (2016) The autophagy machinery controls cell death switching between apoptosis and necroptosis the autophagy machinery controls cell death switching between apoptosis and necroptosis. Dev Cell 37:337–349. https://doi.org/10.1016/j.devcel.2016.04.018

Gowrishankar S, Yuan P, Wu Y et al (2015) Massive accumulation of luminal protease-deficient axonal lysosomes at Alzheimer's

disease amyloid plaques. Proc Natl Acad Sci U S A 112:E3699–E3708. https://doi.org/10.1073/pnas.1510329112
Gustafson DR, Mcfarlane SI (2018) Epidemiology of type 2 diabetes and dementia. Elsevier Inc.
Hou J, Ju J, Zhang Z et al (2019) Discovery of potent necroptosis inhibitors targeting RIPK1 kinase activity for the treatment of in fl ammatory disorder and cancer metastasis. Cell Death Dis. https://doi.org/10.1038/s41419-019-1735-6
Hu C, Huang Y, Li L (2017) Drp1-dependent mitochondrial fission plays critical roles in physiological and pathological progresses in mammals. Int J Mol Sci 18. https://doi.org/10.3390/ijms18010144
Hu L, Zhang S, Wen H et al (2019) Melatonin decreases M1 polarization via attenuating mitochondrial oxidative damage depending on UCP2 pathway in prorenin-treated microglia. PLoS ONE 14:1–18. https://doi.org/10.1371/journal.pone.0212138
Iannielli A, Bido S, Folladori L et al (2018) Pharmacological inhibition of necroptosis protects from dopaminergic neuronal cell death in Parkinson's disease models. Cell Rep 22:2066–2079. https://doi.org/10.1016/j.celrep.2018.01.089
Jantas D, Chwastek J, Grygier B, Lasoń W (2020) Neuroprotective effects of Necrostatin-1 against oxidative stress-induced cell damage: an involvement of Cathepsin D inhibition. Neurotox Res 37:525–542. https://doi.org/10.1007/s12640-020-00164-6
Jauhari A, Baranov SV, Suofu Y et al (2020) Melatonin inhibits cytosolic mitochondrial DNA-induced neuroinflammatory signaling in accelerated aging and neurodegeneration. J Clin Invest 130:3124–3136. https://doi.org/10.1172/JCI135026
Jeon BT, Jeong EA, Shin HJ et al (2012) Resveratrol attenuates obesity-associated peripheral and central inflammation and improves memory deficit in mice fed a high-fat diet. Diabetes 61:1444–1454. https://doi.org/10.2337/DB11-1498
Jiao J, Wang Y, Ren P et al (2020) Necrosulfonamide ameliorates neurological impairment in spinal cord injury by improving antioxidative capacity. Front Pharmacol 10:1. https://doi.org/10.3389/fphar.2019.01538
Johnson LA, Zuloaga KL, Kugelman TL et al (2016) Amelioration of metabolic syndrome-associated cognitive impairments in mice via a reduction in dietary fat content or infusion of non-diabetic plasma. EBioMedicine 3:26–42. https://doi.org/10.1016/j.ebiom.2015.12.008
Joshi AU, Saw NL, Shamloo M, Mochly-rosen D (2018) Drp1 / Fis1 interaction mediates mitochondrial dysfunction, bioenergetic failure and cognitive decline in Alzheimer's disease. 9:6128–6143
Junyi P, Siou L, Simeng W et al (2022) Pathogenesis and research progress of diabetes and cognitive impairment. J Clin Rev Case Reports 7:82
Jurga AM, Paleczna M, Kuter KZ (2020) Overview of general and discriminating markers of differential microglia phenotypes. Front Cell Neurosci 14:1–18. https://doi.org/10.3389/fncel.2020.00198
Kang S, Kim C, Jung H et al (2017) Neuropharmacology Agmatine ameliorates type 2 diabetes induced-Alzheimer's disease-like alterations in high-fat diet-fed mice via reactivation of blunted insulin signalling. Neuropharmacology 113:467–479. https://doi.org/10.1016/j.neuropharm.2016.10.029
Karch J, Kanisicak O, Brody MJ et al (2015) Necroptosis interfaces with MOMP and the MPTP in mediating cell death. 1–12. https://doi.org/10.1371/journal.pone.0130520
Kim DY, Kim SR, Jung UJ (2020) Myricitrin ameliorates hyperglycemia, glucose intolerance, hepatic steatosis, and inflammation in high-fat diet/streptozotocin-induced diabetic mice. Int J Mol Sci 21. https://doi.org/10.3390/ijms21051870
Kim JY, Lee HJ, Lee SJ et al (2017) Palmitic Acid-BSA enhances Amyloid-β production through GPR40-mediated dual pathways in neuronal cells: Involvement of the Akt/mTOR/HIF-1α and Akt/NF-κB pathways. Sci Rep 7:1–16. https://doi.org/10.1038/s41598-017-04175-w
Kodali M, Attaluri S, Madhu LN et al (2021) Metformin treatment in late middle age improves cognitive function with alleviation of microglial activation and enhancement of autophagy in the hippocampus. Aging Cell 20:e13277. https://doi.org/10.1111/acel.13277
Kuhad A, Bishnoi M, Tiwari V, Chopra K (2009) Suppression of NF-κβ signaling pathway by tocotrienol can prevent diabetes associated cognitive deficits. Pharmacol Biochem Behav 92:251–259. https://doi.org/10.1016/J.PBB.2008.12.012
Li C, Casanueva O (2016) Epigenetic inheritance of proteostasis and ageing. Essays Biochem 60:191–202. https://doi.org/10.1042/EBC20160025
Li L, Tong A, Zhang Q et al (2021) The molecular mechanisms of MLKL-dependent and MLKL-independent necrosis. J Mol Cell Biol 13:3–14. https://doi.org/10.1093/JMCB/MJAA055
Li PA, Hou X, Hao S (2017) Mitochondrial biogenesis in neurodegeneration. J Neurosci Res 95:2025–2029. https://doi.org/10.1002/jnr.24042
Lin CF, Liu HC, Lin SY (2022) Kidney function and risk of physical and cognitive impairment in older persons with type 2 diabetes at an outpatient clinic with geriatric assessment implementation. Diabetes, Metab Syndr Obes Targets Ther 15:79. https://doi.org/10.2147/DMSO.S341935
Liu S, Li Y, Choi HMC (2018) Lysosomal damage after spinal cord injury causes accumulation of RIPK1 and RIPK3 proteins and potentiation of necroptosis. Cell Death Dis 1–14. https://doi.org/10.1038/s41419-018-0469-1
Liu Y, Fu X, Lan N et al (2014) Luteolin protects against high fat diet-induced cognitive deficits in obesity mice. Behav Brain Res 267:178–188. https://doi.org/10.1016/j.bbr.2014.02.040
Lu J, Sun Z, Fang Y et al (2019) Melatonin suppresses microglial necroptosis by regulating deubiquitinating enzyme A20 after intracerebral hemorrhage. Front Immunol 10:1360. https://doi.org/10.3389/FIMMU.2019.01360/BIBTEX
Lu XLS, Gang HW, He LY et al (2018) Effects of the fenugreek extracts on high-fat diet-fed and streptozotocin-induced type 2 diabetic mice. 68–73. https://doi.org/10.1002/ame2.12004
Marwarha G, Claycombe K, Schommer J et al (2016) Palmitate-induced Endoplasmic Reticulum stress and subsequent C/EBPα Homologous Protein activation attenuates leptin and Insulin-like Growth Factor 1 expression in the brain. Cell Signal 28:1789. https://doi.org/10.1016/J.CELLSIG.2016.08.012
Melo HM, Seixas da Silva G da S, Sant'Ana MR et al (2020) Palmitate is increased in the cerebrospinal fluid of humans with obesity and induces memory impairment in mice via pro-inflammatory TNF-α. Cell Rep 30:2180-2194.e8. https://doi.org/10.1016/j.celrep.2020.01.072
Nunez J (2008) Morris water maze experiment. 19–21. https://doi.org/10.3791/897
Panyawattanakit C, Wongpradit W, Kanhasing R, Kulalert P (2022) Cognitive impairment and associated factors among older adults with diabetes in a suburban primary health center in Thailand. Dement Geriatr Cogn Disord 51:175–181. https://doi.org/10.1159/000524132
Paolicelli R, Sierra A, Stevens B et al (2022) Defining microglial states and nomenclature: a roadmap to 2030. SSRN Electron J. https://doi.org/10.2139/SSRN.4065080
Park G, Lee JY, Han HM et al (2021) Ablation of dynamin-related protein 1 promotes diabetes-induced synaptic injury in the hippocampus. Cell Death Dis. https://doi.org/10.1038/s41419-021-03723-7
Park KA, Jin Z, Lee JY et al (2020) Long-lasting exendin-4 fusion protein improves memory deficits in high-fat diet/

streptozotocin-induced diabetic mice. Pharmaceutics 12:1–18. https://doi.org/10.3390/pharmaceutics12020159
Patková J, Anděl M, Trnka J (2014) Palmitate-induced cell death and mitochondrial respiratory dysfunction in myoblasts are not prevented by mitochondria-targeted antioxidants. Cell Physiol Biochem 33:1439–1451. https://doi.org/10.1159/000358709
Preeti K, Sood A, Fernandes V (2021) Metabolic regulation of glia and their neuroinflammatory role in Alzheimer's disease. Cell Mol Neurobiol. https://doi.org/10.1007/s10571-021-01147-7
Qing W, Li F, Wang X et al (2018) Inhibiting RIP1 improves chronic stress-induced cognitive impairments in D -galactose-induced aging mice. 12:1–11. https://doi.org/10.3389/fnbeh.2018.00234
Rai U, Kosuru R, Prakash S et al (2019) Tetramethylpyrazine alleviates diabetic nephropathy through the activation of Akt signalling pathway in rats. Eur J Pharmacol 865:172763. https://doi.org/10.1016/J.EJPHAR.2019.172763
Remijsen Q, Goossens V, Grootjans S et al (2014) Depletion of RIPK3 or MLKL blocks TNF-driven necroptosis and switches towards a delayed RIPK1 kinase-dependent apoptosis. 5:e1004–8. https://doi.org/10.1038/cddis.2013.531
Riederer P, Korczyn AD, Ali SS et al (2017) The diabetic brain and cognition. J Neural Transm 124:1431–1454. https://doi.org/10.1007/s00702-017-1763-2
Roberts JZ, Crawford N, Longley DB (2022) The role of ubiquitination in apoptosis and necroptosis. Cell Death Differ 29:272–284. https://doi.org/10.1038/s41418-021-00922-9
Rodriguez DA, Weinlich R, Brown S et al (2015) Characterization of RIPK3-mediated phosphorylation of the activation loop of MLKL during necroptosis. Cell Death Differ 231(23):76–88. https://doi.org/10.1038/cdd.2015.70
Rollins CPE, Gallino D, Kong V et al (2019) Contributions of a high-fat diet to Alzheimer's disease-related decline: a longitudinal behavioural and structural neuroimaging study in mouse models. NeuroImage Clin 21:101606. https://doi.org/10.1016/j.nicl.2018.11.016
Rom S, Zuluaga-Ramirez V, Gajghate S et al (2019) Hyperglycemia-driven neuroinflammation compromises BBB leading to memory loss in both diabetes mellitus (DM) type 1 and type 2 mouse models. Mol Neurobiol 56:1883–1896. https://doi.org/10.1007/s12035-018-1195-5
Rothaug M, Stroobants S, Schweizer M et al (2015) LAMP-2 deficiency leads to hippocampal dysfunction but normal clearance of neuronal substrates of chaperone-mediated autophagy in a mouse model for Danon disease. Acta Neuropathol Commun 3:6. https://doi.org/10.1186/s40478-014-0182-y
Salvadores N, Moreno-Gonzalez I, Gamez N et al (2022) Aβ oligomers trigger necroptosis-mediated neurodegeneration via microglia activation in Alzheimer's disease. Acta Neuropathol Commun 10. https://doi.org/10.1186/S40478-022-01332-9
Schmued LC, Stowers CC, Scallet AC, Xu L (2005) Fluoro-Jade C results in ultra high resolution and contrast labeling of degenerating neurons. Brain Res 1035:24–31. https://doi.org/10.1016/j.brainres.2004.11.054
Sen T, Saha P, Gupta R et al (2020) Aberrant ER stress induced neuronal-IFNβ elicits white matter injury due to microglial activation and T-Cell infiltration after TBI. J Neurosci 40:424–446. https://doi.org/10.1523/JNEUROSCI.0718-19.2019
Sharma D, Verma S, Vaidya S et al (2018) Recent updates on GLP-1 agonists: Current advancements & challenges. Biomed Pharmacother 108:952–962. https://doi.org/10.1016/J.BIOPHA.2018.08.088
Sharoar MG, Palko S, Ge Y et al (2021) Accumulation of saposin in dystrophic neurites is linked to impaired lysosomal functions in Alzheimer's disease brains. Mol Neurodegener 16:1–17. https://doi.org/10.1186/s13024-021-00464-1
Spinelli M, Fusco S, Mainardi M et al (2017) Brain insulin resistance impairs hippocampal synaptic plasticity and memory by increasing GluA1 palmitoylation through FoxO3a. Nat Commun 8:2009–2009. https://doi.org/10.1038/S41467-017-02221-9
Sun L, Wang H, Wang Z et al (2012) Mixed lineage kinase domain-like protein mediates necrosis signaling downstream of RIP3 kinase. Cell 148:213–227. https://doi.org/10.1016/j.cell.2011.11.031
Takechi R, Lam V, Brook E et al (2017) Blood-brain barrier dysfunction precedes cognitive decline and neurodegeneration in diabetic insulin resistant mouse model : an implication for causal link. 9:1–12. https://doi.org/10.3389/fnagi.2017.00399
Takeda S, Sato N, Uchio-Yamada K et al (2010) Diabetes-accelerated memory dysfunction via cerebrovascular inflammation and Aβ deposition in an Alzheimer mouse model with diabetes. Proc Natl Acad Sci U S A 107:7036–7041. https://doi.org/10.1073/PNAS.1000645107/SUPPL_FILE/PNAS.201000645SI.PDF
Thangavel R, Kempuraj D, Zaheer S et al (2017) Glia maturation factor and mitochondrial uncoupling proteins 2 and 4 expression in the temporal cortex of Alzheimer's disease brain. Front Aging Neurosci 9:1–10. https://doi.org/10.3389/fnagi.2017.00150
Urso CJ, Zhou H (2021) Palmitic acid lipotoxicity in microglia cells is ameliorated by unsaturated fatty acids. Int J Mol Sci 22:1–18. https://doi.org/10.3390/ijms22169093
Weber K, Roelandt R, Bruggeman I et al (2018) Nuclear RIPK3 and MLKL contribute to cytosolic necrosome formation and necroptosis. Commun Biol 11(1):1–13. https://doi.org/10.1038/s42003-017-0007-1
Wolf A, Bauer B, Abner EL et al (2016) A comprehensive behavioral test battery to assess learning and memory in 129S6/ Tg2576 mice. PLoS ONE 11:1–23. https://doi.org/10.1371/journal.pone.0147733
Xu D, Jin T, Zhu H et al (2018) Inflammation during development and in aging article TBK1 suppresses RIPK1-driven apoptosis and inflammation during development and in aging. Cell 1–15. https://doi.org/10.1016/j.cell.2018.07.041
Xu H, Du X, Liu G et al (2019) The pseudokinase MLKL regulates hepatic insulin sensitivity independently of in fl ammation. Mol Metab 23:14–23. https://doi.org/10.1016/j.molmet.2019.02.003
Yang S, Lee DK, Shin J et al (2017) Nec- 1 alleviates cognitive impairment with reduction of A b and tau abnormalities in. 9:61–77. https://doi.org/10.15252/emmm.201606566
Yao Q, Feng M, Yang B et al (2018) Effects of ovarian hormone loss on neuritic plaques and autophagic flux in the brains of adult female APP/PS1 double-transgenic mice. Acta Biochim Biophys Sin (shanghai) 50:447–455. https://doi.org/10.1093/abbs/gmy032
Yin C, Zhang Q, Zhao J et al (2022) Necrostatin-1 against sevoflurane-induced cognitive dysfunction involves activation of BDNF/TrkB pathway and inhibition of necroptosis in aged rats. Neurochem Res 474(47):1060–1072. https://doi.org/10.1007/S11064-021-03505-9
Zhang X, Dowling JP, Zhang J (2019) RIPK1 can mediate apoptosis in addition to necroptosis during embryonic development. Cell Death Dis. https://doi.org/10.1038/s41419-019-1490-8
Zhang Y, Li M, Li X et al (2020) Catalytically inactive RIP1 and RIP3 deficiency protect against acute ischemic stroke by inhibiting necroptosis and neuroinflammation. Cell Death Dis 117(11):1–10. https://doi.org/10.1038/s41419-020-02770-w

Zhao X, Wang H, Sun G et al (2015) Neuronal Interleukin-4 as a Modulator of Microglial Pathways and Ischemic Brain Damage. J Neurosci 35:11281. https://doi.org/10.1523/JNEUROSCI.1685-15.2015

Zhou H, Li D, Zhu P et al (n.d.) Inhibitory effect of melatonin on necroptosis via repressing the Ripk3-PGAM5-CypD-mPTP pathway attenuates cardiac microvascular ischemia reperfusion injury. 0–3. https://doi.org/10.1111/jpi.12503

Zilliox LA, Chadrasekaran K, Kwan JY, Russell JW (2016) Diabetes and cognitive impairment. Curr Diab Rep 16:87. https://doi.org/10.1007/S11892-016-0775-X

Zou C, Mifflin L, Hu Z et al (2020) Reduction of mNAT1/hNAT2 contributes to cerebral endothelial necroptosis and Aβ accumulation in Alzheimer's disease. Cell Rep 33:108447. https://doi.org/10.1016/j.celrep.2020.108447

Zuo W, Liu Z, Yan F et al (2019) Hyperglycemia abolished Drp-1-mediated mitophagy at the early stage of cerebral ischemia. Eur J Pharmacol 843:34–44. https://doi.org/10.1016/j.ejphar.2018.11.011